

Turbulence Inhibits Planetesimal Formation in Class 0/I Disks Subject to Infall

DANIEL CARRERA ¹, ABIGAIL DAVENPORT,¹ JACOB B. SIMON ¹, HANS BAEHR ², TIL BIRNSTIEL,^{3,4}
CASSANDRA HALL ², DAVID REA,¹ AND SEBASTIAN MARKUS STAMMLER ³

¹*Department of Physics and Astronomy, Iowa State University, Ames, IA, 50010, USA*

²*Department of Physics and Astronomy, The University of Georgia, Athens, GA 30602, USA*

³*University Observatory, Faculty of Physics, Ludwig-Maximilians-Universität München, Scheinerstr. 1, 81679 Munich, Germany*

⁴*Max Planck Institute for Solar System Research, Justus-von-Liebig-Weg 3, Göttingen, 37077, Germany*

Submitted to ApJ

ABSTRACT

There is growing evidence that planet formation begins early, within the $\lesssim 1$ Myr Class 0/I phase, when infall dominates disk dynamics. Our goal is to determine if Class 0/I disks reach the conditions needed to form planetesimals (~ 100 km planet building blocks) by the streaming instability (SI). We focus on a recent suggestion that early infall causes an “inflationary” phase in which dust grains are advected outward. We modified the `DustPy` code to build a 1D disk that includes dust evolution, infall, and heating and cooling sources. We ran six models and examined the implications for the SI, taking into account recent works on how the SI responds to external turbulence. In line with other works, we find that grains are advected outward, which leads to “advection-condensation-drift” loop that greatly enhances the dust density at the water snowline. However, we do not see this process at the silicate line. Instead, we find a new pile up at the edge of the expanding disk. However, despite these localized enhancements, even a modest amount of turbulence ($\alpha = 10^{-3}$) leaves planetesimal formation far out of reach. The midplane dust-to-gas ratio is at least an order of magnitude below the SI threshold, even taking into account recent results on how dust coagulation boosts the SI. For planetesimals to form in the Class 0/I phase may require a way to transport angular momentum without turbulence (e.g., disk winds) or a non-SI mechanism to form planetesimals.

Keywords: accretion disks – protoplanetary disks – planets and satellites: formation

1. INTRODUCTION

Planetesimals are $\sim 1 - 1,000$ km bodies that are the building blocks of terrestrial planets and the cores of giant planets (Kokubo & Ida 1996, 2000). As such, they are key to understanding the properties and chemical compositions of planetary bodies (e.g., Chambers 2001; Morbidelli et al. 2000; Öberg & Wordsworth 2019).

Despite their importance, the origin of planetesimals is arguably the largest gap in our understanding of planet formation. Theoretical models by Johansen et al. (2007) and Cuzzi et al. (2008), together with evidence from the size frequency distribution of present-day asteroids and

the cratering record of Vesta (Morbidelli et al. 2009), and the ubiquity of equal-size binaries in the Kuiper belt (Nesvorný et al. 2010; Fraser et al. 2017) lead to a growing consensus that planetesimals likely formed through the gravitational collapse of a dense cloud of mm-cm size particles, skipping across the intermediate sizes. Among the proposed mechanisms, the streaming instability (SI, Youdin & Goodman 2005; Johansen & Youdin 2007; Youdin & Johansen 2007) has drawn the most attention in recent years. One recent success for the SI is the reproduction of the obliquity and angular momentum distributions of trans-Neptunian binaries (Nesvorný et al. 2019, 2021).

However, many crucial challenges remain for the SI. The root problem is that the conditions needed to trigger the SI (Carrera et al. 2015; Yang et al. 2017; Li & Youdin

2021; Lim et al. 2025) seem to require larger grains and/or higher solid-to-gas ratios than predicted by dust evolution models. Carrera et al. (2017)’s attempt to reach the conditions for the SI through disk photoevaporation only resulted in late formation of planetesimals (too late to form planets). Pressure bumps have long been considered promising locations for the SI (e.g., Lau et al. 2022), as they concentrate solids (e.g., Taki et al. 2016) and reduce the radial pressure gradient, which is a key parameter for the SI (Sekiya & Onishi 2018). While work by Carrera et al. (2021) showed promising results in the case of relatively large particles, a follow-up study by Carrera & Simon (2022) with smaller particles uncovered a new problem: Even if the conditions for the SI are nominally met in a pressure bump, planetesimals may still fail to form for small (possibly more realistic) particle sizes because the growth timescale of the SI may be longer than the crossing time of solids across the bump, at least in the case of pressure bumps that slow down the drifting particles without halting their drift completely.

1.1. Streaming Instability in Class 0/I Disks?

This paper is another attempt to find a realistic scenario in which a circumstellar disk triggers the SI to form planetesimals, inspired by recent work by Morbidelli et al. (2022), Marschall & Morbidelli (2023), and Estrada & Umurhan (2023).

There is growing evidence that planet formation starts early. For one, Class II disks may not contain enough dust mass to reproduce the observed exoplanet population (Manara et al. 2018 but see Mulders et al. 2021 and Liu et al. 2024), suggesting that, at a minimum, the process of converting dust into planetesimals occurs in the Class 0/I stage. Furthermore, the ubiquity of dust rings in ALMA images suggests that giant planet cores also form early, if indeed these rings are the result of giant planets opening gaps along their orbits. Finally, within the context of our own solar system, there is meteoritic evidence that Jupiter’s core formed within the first 1 Myr of the birth of the solar nebula (Kruijjer et al. 2017; Desch et al. 2018).

Recently, Morbidelli et al. (2022) suggested a scenario in which planetesimals form, via the SI, during an early “inflationary” stage of a Class 0/I disk. The Class 0/I stage corresponds to the time when the star and disk are shrouded by a gas envelope, and infall from the envelope plays an important role in the disk dynamics. Morbidelli et al. (2022) argue that, due to magnetic braking, the infall is deposited close to the central star, causing the disk to spread viscously. They built a simple 1D disk with a “two population” model for dust evolution (Birnstiel

et al. 2012). They found that the gas outflow combines with condensation/sublimation and radial drift to produce a significant pile up of material. The proposed mechanism is that solids, as well as silicate and water vapor, are advected outward by the gas, cross the condensation line, form large solids, and then drift back in. Marschall & Morbidelli (2023) also see this cyclical process, and additionally report a significant pile up of material.

In contrast, earlier work (Birnstiel et al. 2010) conducted 1D simulations of a protoplanetary disk with infall, following the solid-body rotation infall model of Shu (1977). While their models show regions where dust is advected outward, they do not report the cyclical process suggested by Morbidelli et al. (2022). More recently, Estrada & Umurhan (2023) conducted their own investigation of the SI in a 1D disk, using a model of dust growth with multiple dust species, and found a nearly opposite result: the solid concentration, and especially the particle sizes, are not nearly high enough to meet any of the proposed criteria for the SI (Carrera et al. 2015; Yang et al. 2017; Li & Youdin 2021; Lim et al. 2025).

Why did these works reach opposite conclusions? The most notable difference between them is that Morbidelli et al. (2022) and Marschall & Morbidelli (2023) have an inflationary disk, but a simple treatment of dust growth, while Estrada & Umurhan (2023) have a sophisticated model for dust growth, but not an inflationary disk. At the same time, Birnstiel et al. (2010) had both, but did not explore the implications for the SI.

It is our hope that our work will help settle this issue. Our contribution is a 1D disk model that has both a sophisticated treatment of dust evolution, built on top of `DustPy` (Stammler & Birnstiel 2022), but adopting the exact same inflationary model of Morbidelli et al. (2022) and Marschall & Morbidelli (2023). In addition,

- We also explore a wider portion of the parameter space: We test varying stellar masses and we examine some of the simplifications in the thermal model of Marschall & Morbidelli (2023).
- We added a prescription for the effect of disk self-gravity on angular momentum transport (though this turned out to be a negligible effect in the disk regions that we are interested in).
- Importantly, we take into account recent works that explore how the SI behaves under turbulence (Lim et al. 2024) as well as a feedback mechanism between dust growth and the SI (Carrera et al. 2025). Before Lim et al. (2024), the SI criteria

have relied heavily on 2D simulations where the SI itself is the only source of turbulence.

This paper is organized as follows. Our experiment and numerical model are detailed in section §2. Results are presented in section §3, followed by a discussion and implications in section §4. Lastly, we summarize and conclude in section §5.

2. METHODS

We modified `DustPy` (Stammler & Birnstiel 2022) to make a 1D model of a Class 0/I disk. `DustPy` solves the gas and dust evolution equations of a 1D axisymmetric circumstellar disk, and has been used often to model Class II disks. To adapt `DustPy` to a Class 0/I disk we added infall from the surrounding envelope, we compute the thermal evolution of the disk using the flux-limited diffusion model, and we added prescriptions for heating due to infall, turbulent viscosity, and gravitoturbulence. Since the early disk is very hot, we added the silicate condensation front in addition to the water snowline. In the rest of this section we describe each component in turn.

2.1. Structure of a Class 0/I Disk

The surface density Σ of a circumstellar accretion disk is primarily determined by its temperature T and by angular momentum transport. For instance, the accretion rate of a steady-state disk is

$$\dot{M} = 3\pi\nu\Sigma \quad (1)$$

where ν is the disk viscosity, which quantifies angular momentum transport. It is commonly expressed as an “alpha viscosity” $\nu = \alpha c_s H$ (Shakura & Sunyaev 1973) where c_s is the sound speed and $H = c_s/\Omega$ is the vertical pressure scale height of the gas and Ω is the Keplerian angular frequency.

While disk self-gravity does not play a significant role in the inner disk, in the outer disk it can be an important component of angular momentum transport, can cause large-scale spiral structures, and can even lead to disk fragmentation (Gammie 2001). The strength of self-gravity is quantified by Toomre (1964)’s Q stability parameter

$$Q \equiv \frac{\Omega c_s}{\pi G \Sigma}, \quad (2)$$

where G is the gravitational constant. If the disk lacks a sufficient source of heating, it will cool down until $Q \approx 1$, at which point gravitational instabilities generate spiral shocks that both heat the disk (Goldreich & Lynden-Bell

1965; Durisen et al. 2007) and contribute to outward angular momentum transport (Lin & Pringle 1987; Laughlin & Bodenheimer 1994; Lodato & Rice 2005; Cossins et al. 2009) allowing the disk to accrete.

For $M_{\text{disk}} < 0.5M_\star$ (M_{disk} and M_\star are the disk and stellar masses, respectively) the disk settles into a quasi-steady state with $Q \approx 1 - 2$ (Paardekooper et al. 2011) where the angular momentum transport due to self-gravity can be treated as a local process with an effective α (Lodato & Rice 2005; Rice 2016). For a viscous disk in thermal equilibrium, Shakura & Sunyaev (1973)’s α parameter can be related to the cooling time t_{cool} via Gammie (2001)

$$\alpha = \frac{4}{9\gamma(\gamma - 1)} (\Omega t_{\text{cool}})^{-1} \quad (3)$$

where γ is the adiabatic index and t_{cool} is the cooling timescale.

For a more massive disk with $M_{\text{disk}} \approx M_\star$, the disk forms a series of recurrent grand-design spirals with a dominant $m = 2$ mode. While accretion is clearly non-local in this regime, Lodato & Rice (2005) found that the effective α during the spiral episodes is not much larger during periods of low-spiral activity, and both values lie close to the value expected based on the balance between heating and cooling. Furthermore, the spiral structures are short-lived, as they form and dissipate on an orbital timescale. Therefore, Rice (2016) suggest that for M_{disk}/M_\star approaching unity the local approximation is still valid “in a time-averaged sense” (see also Xu & Kunz 2021 and Béthune et al. 2021). In practice, our simulations never get close to $M_{\text{disk}}/M_\star \sim 1$; our simulations peak at $M_{\text{disk}}/M_\star < 0.15$ after $\sim 10^5$ yr.

2.2. The Experiment

Table 1. Our six simulations span two initial stellar masses $M_{\star,0}$ and three infall models: A classic model (Shu 1977), one where infall has a low angular momentum due to magnetic braking (Morbidelli et al. 2022), and a “Soft Landing” where infall additionally loses kinetic energy before the infall reaches the disk surface (this work).

	$M_{\star,0}$	Infall model
Classic-M05	0.5	Classic
Classic-M03	0.3	Classic
Low-Ang-M05	0.5	Low Ang Momentum
Low-Ang-M03	0.3	Low Ang Momentum
Soft-Land-M05	0.5	Soft Landing (this work)
Soft-Land-M03	0.3	Soft Landing (this work)

Our experiment consists of three infall models and six simulations (Table 1). We adopt the two infall mod-

els of [Marschall & Morbidelli \(2023\)](#), and add a third “Soft Landing” model where we assume that the infall loses most of its gravitational potential energy before it reaches the disk surface (see below for more details). In all cases, the total gas infall rate is

$$\dot{M}(t) = \frac{M_{\odot} - M_{\star,0}}{t_{\text{infall}}} \exp\left[-\frac{t}{t_{\text{infall}}}\right] \quad (4)$$

where $M_{\star,0}$ is the initial stellar mass (either 0.5 or $0.3 M_{\odot}$) and we follow [Marschall & Morbidelli \(2023\)](#) in setting $t_{\text{infall}} = 10^5 \text{yr}$. Let r_+ and r_- be the boundaries of a radial grid cell and let R_c be the centrifugal radius.

$$\dot{M}(r, t) = \left[\left(1 - \sqrt{\frac{r_-}{R_c}}\right)^{1/2} - \left(1 - \sqrt{\frac{r_+}{R_c}}\right)^{1/2} \right] \dot{M}(t) \quad (5)$$

for $r_+ < R_c$ and 0 otherwise. Infall inside 0.05AU is assumed to fall directly onto the central star, and is added to the stellar mass on every timestep. We also track the disk accretion rate and add the accreted gas mass to the star as well. To shorten the simulation time, we set the inner edge of the disk to $r_{\text{in}} = 0.25 \text{AU}$ for the $M_{\star,0} = 0.5 M_{\odot}$ runs and 0.20AU for the $M_{\star,0} = 0.3 M_{\odot}$ and scale $\dot{M}(r, t)$ accordingly so that $\sum_r \dot{M}(r, t) = \dot{M}(t)$. Our choices of r_{in} reflect the trade-off between computing speed and resolving the important regions of the disk. The runs with $M_{\star,0} = 0.3 M_{\odot}$ ran slightly faster, which allowed us to choose a smaller r_{in} . Lastly, there is one grid cell with $r_- < R_c < r_+$. That is the cell where $\dot{M}(r)$ is highest, so we were careful to account for that cell accurately (we replace r_+ with R_c in Equation 5). In the end, all the infall is accounted for, and in the long run, the stellar mass converges to exactly $1 M_{\odot}$. Figure 1 shows $\dot{M}(r, t)$ for a sample snapshot.

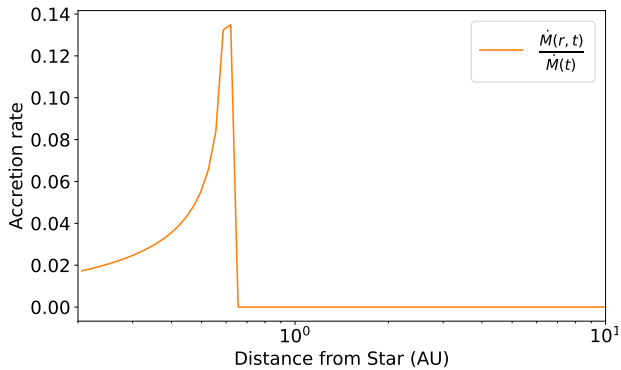


Figure 1. Infall rate $\dot{M}(r, t)$ for a sample snapshot (the **Log-Ang-M03** model at $t = 10^4 \text{yr}$). The infall rate peaks at R_c . See Equation 5 and the main text.

Aside from r_{in} , our models are distinguished from each other by how we calculate R_c and how much energy is deposited onto the disk. Our infall models are:

1. **Classic:** Based on [Shu \(1977\)](#), we model the gas cloud as a rigidly rotating sphere and is ([Marschall & Morbidelli 2023](#))

$$R_c = 53 \text{AU} \left(\frac{\omega}{10^{-14} \text{s}^{-1}} \right)^2 \left(\frac{T}{10 \text{K}} \right)^{-4} \left(\frac{M_{\text{tot}}}{M_{\odot}} \right)^3 \quad (6)$$

where $\omega = 9 \times 10^{-15} \text{s}^{-1}$ is the angular velocity of the cloud, $T = 15 \text{K}$ is its temperature, and M_{tot} is the total mass of the star-disk system. The energy deposited onto the disk is

$$\dot{Q}_{\text{infall}} = \frac{1}{2} \frac{GM_{\star}(t)\dot{M}(r)}{r} \quad (7)$$

where G is the gravitational constant. This model assumes that only half of the potential energy of the gas is injected into the disk and the rest is lost during the infall phase.

2. **Low Ang Momentum:** In the scenario proposed by [Morbidelli et al. \(2022\)](#), the infalling material loses angular momentum due to magnetic braking.

$$R_c = \frac{0.35 \text{AU}}{\sqrt{M_{\star}(t)}} \quad (8)$$

and \dot{Q}_{infall} follows Equation 7.

3. **Soft Landing:** Same R_c as in the **Low-Ang** model, but we additionally assume that only 1% of the potential energy in the cloud makes its way onto the disk surface.

$$\dot{Q}_{\text{infall}} = 0.01 \frac{GM_{\star}(t)\dot{M}(r)}{r} \quad (9)$$

This model is motivated by recent 3D simulations of disk formation ([Mauxion et al. 2024](#)); these studies indicate that the infall may lose much of its energy before landing on the surface of the disk. However, they did not follow the energy evolution in the system, nor did they resolve the inner few AU, making it difficult to quantify precisely how much energy is lost during the infall phase prior to the gas reaching the inner disk. Thus, we make a conservative estimate that 99% of potential energy is lost before landing on the disk (e.g., through Poynting flux).

A related issue is that heating from \dot{Q}_{infall} occurs at the surface of the disk, not the midplane. [Morbidelli et al. \(2022\)](#) use a simple relation to link surface and midplane temperatures

$$T_{\text{surf}}^4 = \frac{4}{3} \frac{2T^4}{\kappa\Sigma} \quad (10)$$

where κ is the opacity (we use [Bell & Lin \(1994\)](#) opacities). This formula is valid for an optically thick disk heated at the midplane. [Morbidelli et al. \(2022\)](#)'s model computes the temperature as if all heating and cooling occurs at the midplane (see §2.6) and Equation 10 links T and T_{surf} , which sets the cooling rate from black-body radiation. However, \dot{Q}_{infall} occurs at the surface, not the midplane, and that heat has to propagate inward. As a result, Equation 10 may overestimate the contribution from \dot{Q}_{infall} . The **Soft Landing** model lowers \dot{Q}_{infall} by 99% in order to determine how this uncertainty impacts the model results. It is an important test for the robustness of the other models in this work.

2.3. Gas Evolution

`DustPy` uses the adiabatic sound speed

$$c_s = \sqrt{\frac{\gamma k_B T}{\mu}} \quad (11)$$

where γ is the adiabatic index, k_B is the Boltzmann constant, and μ is the mean molecular weight of the gas. We use $\gamma \equiv 1.4$ and $\mu \equiv 2.3 \text{g mol}^{-1}$ for the entire disk, making the approximation that μ remains constant across condensation lines.

`DustPy` solves the viscous evolution of the gas surface density Σ via the viscous advection-diffusion equation

$$\frac{\partial \Sigma}{\partial t} + \frac{1}{r} \frac{\partial}{\partial r} (r v_r \Sigma) = S_{\text{ext}} \quad (12)$$

where r is the radial coordinate (i.e., the distance from the star), v_r is the radial velocity of the gas, and S_{ext} is an external source term that we use to model infall

$$S_{\text{ext}}(r, t) = \frac{\dot{M}(r, t)}{\pi(r_+^2 - r_-^2)}. \quad (13)$$

For a viscous disk, the radial velocity is given by ([Lynden-Bell & Pringle 1974](#))

$$v_r = -\frac{3}{\Sigma\sqrt{r}} \frac{\partial}{\partial r} (\nu\Sigma\sqrt{r}) \quad (14)$$

By default, `DustPy` uses the α -prescription for disk viscosity $\nu = \alpha c_s H$ ([Shakura & Sunyaev 1973](#)). One can

express the contribution of gravitoturbulence to angular momentum transport as an additional term α_{gt} (detailed in §2.4). Therefore, we write

$$\nu = \alpha_{\text{tot}} c_s H \quad (15)$$

$$\alpha_{\text{tot}} = \alpha_{\text{vis}} + \alpha_{\text{gt}}, \quad (16)$$

where $\alpha_{\text{vis}} \equiv 10^{-3}$ is the baseline turbulent α . Equation 3 ties α to viscous heating. In our model, viscous heating is computed from α_{tot} . Finally, note that with our choice of infall timescale and α_{vis} , we reach a stellar mass of $0.9M_\odot$ and an outer radius of ~ 50 au in 500 kyr. Thus, we are confident that these parameters are reasonable for a viscously accreting disk with infall.

2.4. Disk Self-Gravity

We only consider self-gravity as a potential source of heating and angular momentum transport, and not as a source for turbulence-induced collisions between grains (as we describe below). If the disk can form spiral structures, [Rice et al. \(2004\)](#) suggests that “intermediate sized particles” (St $\sim 0.5 - 10$) can concentrate strongly inside. This can be safely ignored in our model because our grains are much smaller than St ~ 0.5 and the disk is not massive enough to form global $m = 2$ spiral structures ($M_{\text{disk}}/M_\star = 0.14$ for our most massive disk, which will not form such low m structures; [Kratler & Lodato 2016](#)). The model with the most massive disk is `Classic-M05`, which reaches a maximum disk mass of $M_{\text{disk}} = 0.11M_\odot$ within 50 AU. This is also the least stable disk, with Toomre parameter of $Q = 1.67$. Figure 2 shows the minimum Toomre Q for our *-M05 runs — the values for the *-M03 runs are similar.

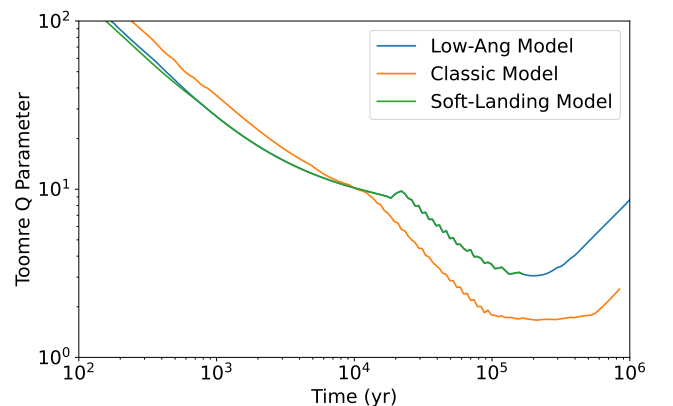


Figure 2. Smallest Toomre Q parameter for our *-M05 simulations. The Q values for the *-M03 runs are similar.

Our treatment of disk self-gravity follows the approach of [Rafikov \(2015\)](#), who used thermal balance arguments

to derive an expression for an “effective α ” that captures the contribution to angular momentum transport due to gravitoturbulence.

$$\alpha_{\text{gt}} = \frac{8}{9} \frac{\sigma(\pi G Q_0)^6}{\tau + \tau^{-1}} \left(\frac{\mu}{k_B}\right)^4 \frac{\Sigma^4}{\Omega^7} \left(1 - \frac{T_{\text{irr}}^4}{T_Q^4}\right) \quad (17)$$

where k_B is the Boltzmann constant, $Q_0 \equiv 1.5$ is the threshold for gravitational instability (GI) suggested by numerical experiments (Cossins et al. 2009, 2010); that value is not exact (e.g. Béthune et al. 2021, shows a density weighted $\langle Q_0 \rangle_\rho \approx 1.2$) but we adopt $Q_0 \equiv 1.5$ to remain consistent with Rafikov (2015). Lastly, T_Q is the critical temperature for GI, which is calculated by setting $Q = Q_0$ in Equation 2,

$$T_Q = \frac{\mu}{k_B} \left(\frac{\pi G Q_0}{\Omega}\right)^2 \Sigma^2. \quad (18)$$

Note that Equation 17 gives a negative value whenever $T_{\text{irr}} > T_Q$, meaning that irradiation is sufficient to bring the disk above $Q = Q_0$. When this occurs, we follow Rafikov (2015) and set $\alpha_{\text{gt}} \equiv 0$, as self-gravity does not play a role under those conditions. In any case, α_{gt} is a component of α that determines both the rate of angular momentum transport and the viscous heating of the disk.

2.5. Dust Evolution

Dust evolution in `DustPy` has three components: dust transport (hydrodynamics), coagulation, and external sources. To account for transport and external sources, `DustPy` solves the advection-diffusion equation for each grain size (denoted by the subscript “d”)

$$\frac{\partial \Sigma_d}{\partial t} + \frac{1}{r} \frac{\partial}{\partial r} \left[r v_{r,d} \Sigma_d - r \Sigma D_d \frac{\partial}{\partial r} \left(\frac{\Sigma_d}{\Sigma} \right) \right] = S_{\text{ext},d} \quad (19)$$

For $S_{\text{ext},d}$, we set the total dust mass infall to

$$\sum_d S_{\text{ext},d} = 0.01 S_{\text{ext}}. \quad (20)$$

The value of each $S_{\text{ext},d}$ is determined by the grain size distribution. After testing we found that the simulations are considerably faster if the dust grains that are falling match the local (i.e., where the infalling dust grains land) grain sizes of the disk, with minimal impact on the simulation results compared to a model in which the infalling grains follow the MRN distribution (Mathis et al. 1977). Models with small grain infall show rapid dust growth and require very small time steps.

The D_d in Equation 19 is the radial diffusivity of the dust, which is assumed to be (Youdin & Lithwick 2007)

$$D_d = \frac{\delta_r c_s H}{1 + \text{St}_d^2}, \quad (21)$$

where $\text{St}_d = t_{\text{stop}} \Omega$ is the Stokes number of a grain with stopping time t_{stop} , and δ_r is the radial diffusion coefficient (see below) The stopping time is determined by the grain’s size a_d and material density ρ_s , and the local gas density. We refer the reader to the `DustPy` documentation for details of how St_d is calculated.

Throughout all our runs we set $\delta_r = \alpha_{\text{vis}}$, thus not including α_{gt} . In other words, we assume that disk self-gravity can contribute to large scale angular momentum transport but that this does not translate into small-scale turbulence that can directly impact the dust. This is a valid assumption for the small ($\text{St}_d \leq 0.1$) grains that we see in our simulations and are likely to exist in circumstellar disks, but for large ($\text{St}_d \geq 1$) grains gravitoturbulence leads to enhanced collision speeds (Shi et al. 2016). Note that `DustPy` assumes isotropic turbulence. Thus, to within a factor of order unity, the turbulent diffusion parameter (i.e., turbulent Mach number squared) $\delta_{\text{turb}} = \delta_r = \delta_z$. Based on our assumption above that $\delta_r = \alpha_{\text{vis}}$, $\delta_{\text{turb}} = \delta_r = \delta_z = \alpha_{\text{vis}}$. Thus, α_{vis} sets our dust scale height.

$$H_d = H \sqrt{\frac{\alpha_{\text{vis}}}{\alpha_{\text{vis}} + \text{St}_d}}. \quad (22)$$

In our model most particles are in the “intermediate” regime, where t_{stop} falls between the turnover timescale of the smallest (t_{small}) and largest (t_{large}) eddies. In this regime, the collision velocity is given by (Ormel & Cuzzi 2007); again equating δ_{turb} and α_{vis} , we have

$$v_{d,\text{turb}} = c_s \sqrt{3\alpha_{\text{vis}} \text{St}_d}. \quad (23)$$

Particles with $t_{\text{stop}} < t_{\text{small}}$ or $t_{\text{stop}} > t_{\text{large}}$ have other expressions for $v_{d,\text{turb}}$ (Ormel & Cuzzi 2007). `DustPy` takes into account not only $v_{d,\text{turb}}$ but also the relative velocities due to Brownian motion and the difference in radial drift velocity for particles with different St . We refer the reader to the `DustPy` documentation for more details.

2.6. Disk Temperature

We use the same method as Morbidelli et al. (2022) to compute the disk temperature, including self-gravity α_{gt} as part of the viscous heating.

$$\dot{Q}_{\text{visc}} = 2\pi r \Delta r \frac{9}{4} \Sigma \nu \Omega^2 \quad (24)$$

where $\nu = \alpha_{\text{tot}} c_s H$ and $\Delta r = r_+ - r_-$ is the width of the grid cell. Next, we include disk cooling due to black body radiation at the surface

$$\dot{Q}_{\text{bb}} = 2 \times 2\pi r \Delta r \sigma_{\text{B}} T_{\text{surf}}^4 \quad (25)$$

where σ_{B} is the Stephan-Boltzmann constant, and T_{surf} is the surface temperature, which is tied to the midplane temperature T by Equation 10.

Lastly, we include the energy flux between adjacent rings using a flux-limited diffusion model. A ring gains or loses energy at a rate $\Delta F = F_+ - F_-$, where F_+ and F_- are the energy fluxes across the exterior and interior cell boundaries respectively.

$$F = (2\pi)^{3/2} \frac{16\lambda\sigma_{\text{B}}}{\kappa\rho} \frac{dT}{dr} T^3 r H \quad (26)$$

where $\rho = \Sigma/(H\sqrt{2\pi})$ is the volume gas density at the midplane and λ is the flux limiter, which we compute using the method of Bitsch et al. (2013)

$$\lambda = \begin{cases} 2/(3 + \sqrt{9 + 10R^2}) & \text{for } R \leq 2 \\ 10/(10R + 9 + \sqrt{81 + 180R}) & \text{for } R > 2 \end{cases} \quad (27)$$

where

$$R = \frac{1}{\rho\kappa} \frac{|\nabla E_R|}{E_R}. \quad (28)$$

and $E_R = 4\sigma_{\text{B}}T^4/c$ is the radiative energy density in the optically thick limit. To estimate κ , E_R , ρ , T , H at the boundaries between adjacent rings, we compute the arithmetic average of their values inside the rings.

With these ingredients, we can compute the change of internal energy ΔQ of a ring over a timestep Δt

$$\Delta Q = \left(\dot{Q}_{\text{infall}} + \dot{Q}_{\text{visc}} - \dot{Q}_{\text{bb}} + \Delta F \right) \Delta t. \quad (29)$$

Then the change in temperature is

$$\Delta T = \frac{\Delta Q}{C_{\text{v}} m_{\text{ring}}} \quad (30)$$

where $m_{\text{ring}} = \pi(r_+^2 - r_-^2)(\Sigma + \Sigma_{\text{d}})$ is the mass of the ring,

$$C_{\text{v}} = \frac{\mathcal{R}}{(\gamma - 1)\mu} \quad (31)$$

is the ring's heat capacity and \mathcal{R} is the gas constant. The stellar irradiation plays an indirect role in that we also assume that the disk temperature cannot fall below that of a passively irradiate disk $T_{\text{irr}} = 115\text{K}(r/\text{AU})^{-3/7}$.

2.7. Snowlines

While the molecular weight of the gas μ is kept fixed across evaporation fronts, we do model how the sticking properties of silicate and icy grains affect their sizes. The standard way to implement snowlines in `DustPy` is by altering the solid fragmentation speed v_{frag} across a temperature threshold; collision speeds below v_{frag} are assumed to lead to grains sticking while those above v_{frag} lead to fragmentation.

We start silicate evaporation at $T = 1,000\text{K}$. `DustPy` does not have a mechanism to track silicate vapor. Thus, to simulate silicate vapor we set v_{frag} to an arbitrary small value ($v_{\text{frag}} = 10 \text{ cm s}^{-1}$) to keep grains small and well-coupled to the gas.

$$v_{\text{frag}} = \begin{cases} 10 \text{ cm s}^{-1} & \text{for } T > 1,000\text{K} \\ 1 \text{ m s}^{-1} & \text{for } 170\text{K} < T \leq 1,000\text{K} \\ 10 \text{ m s}^{-1} & \text{for } 95\text{K} < T \leq 170\text{K} \\ 1 \text{ m s}^{-1} & \text{for } T \leq 95\text{K} \end{cases} \quad (32)$$

The collision velocity that leads to sticking for SiO_2 grains is highly dependent on grain size and morphology (Poppe et al. 2000). Here we adopt $v_{\text{frag}} = 1 \text{ m s}^{-1}$ for silicate grains; this value is commonly used in the literature (e.g., Carrera et al. 2017) and is the sticking threshold for $\sim 1\mu\text{m}$ spherical grains (Poppe et al. 2000; Blum & Wurm 2008).

The sticking behavior of icy grains is less well understood and more complex than silicate grains. Simulations of ice-dust aggregates by Wada et al. (2009) suggest $v_{\text{frag}} \sim 50 \text{ m s}^{-1}$, but Gundlach & Blum (2015) conducted lab experiments of icy grains that suggest a value closer to 10 m s^{-1} . In this investigation we opt for the latter value as the conservative choice. The next complication is that the sticking force is temperature dependent. Musiolik & Wurm (2019) measured the rolling and sticking forces of water and found that just 25K below the condensation line the forces decrease by over an order of magnitude, reducing the sticking velocity by a factor of 32. Then, a follow-up numerical study by Musiolik (2021) suggested that UV irradiation produces a liquid-like shell on icy grains, which may damp collisions. They predict that a shell just a few microns thick would be enough to allow the growth of cm-size clusters of grains.

In an effort to capture the essence of these results, we opted to maintain $v_{\text{frag}} = 10 \text{ m s}^{-1}$ for icy grains over a temperature interval of 75K from the snowline and then lower it to $v_{\text{frag}} = 1 \text{ m s}^{-1}$.

2.7.1. Sidenote On Silicate Vapor

As noted above, `DustPy` does not have a mechanism for tracking multiple vapor species. To mimic the behavior of silicate vapor, we arbitrarily set $v_{\text{frag}} = 10 \text{ cm s}^{-1}$ for $T > 1,000\text{K}$. This makes the silicate grains small and well-coupled to the gas, so that they follow the flow of the gas, just as silicate vapor would, while allowing us to keep track of the silicate mass. When these small grains are advected outward, or the disk cools below $T = 1,000\text{K}$, the increase in v_{frag} mimics silicate condensation. There are two ways that small grains differ from silicate vapor: They are less coupled to the gas, and when they cross the silicate condensation line, instead of condensing (as vapor would) they have to grow gradually by sticking collisions. To quantify how this method may affect our results, we re-ran one of our simulations (`Low-Ang-M05`) with $v_{\text{frag}} = 0.1 \text{ cm s}^{-1}$. We found that the simulation results are identical (except for the “grain size” inside the silicate line) albeit with higher computational cost due to smaller time steps.

In the next section we only present the plots from our initial set of runs, with the knowledge that the larger-than-intended grain sizes for $T > 1,000\text{K}$ do not impact our results.

3. RESULTS

3.1. Inflationary Disk and Infall

Figure 3 shows snapshots at $t = 10^3$ and 10^5 yr of the dust density profile for each of the models with $M_{*,0} = 0.5M_{\odot}$. In all cases we see an expanding disk as it spreads viscously. The `Classic-M05` model, with its larger angular momentum and centrifugal radius, extends further out.

In contrast, the difference between `Low-Ang-M05` and `Soft-Land-M05` is barely discernible at 10^3 yr (the latter has slightly more cm-size grains at ~ 1 AU), and the models are nearly indistinguishable at 10^5 yr. We find that the temperature profile (discussed in Section 3.4) is nearly identical in the two models. Even if we focus on just the heating sources and the earliest times (10^3 yr) we find that Q_{infall} only dominates the heating inside 0.6 AU for `Low-Ang` and in a narrow band between 0.30 and 0.45 AU for `Soft-Land`. In other words, Q_{infall} does not dominate the physics.

[Mauxion et al. \(2024\)](#) showed that infall loses much of its energy before it even reaches the disk surface. When it does, the shock heating at the disk surface needs to propagate down toward the midplane. The detailed physics of this process are beyond the scope of this work. Instead, we simply consider two extreme cases:

- **Low-Ang model:** Assume that 50% of the gravitational potential energy reaches the midplane.

- **Soft-Land model:** Assume that only 1% of the energy reaches the midplane.

The true behavior of infall must lie between these extremes. Figure 4 shows the accretion rate \dot{M} for these two models. It shows that Q_{infall} has a minimal effect on the physics. We do see some positive feedback where Q_{infall} increases the temperature, which adds viscosity since $\nu \propto c_s^2 \propto T$ thus enhancing viscous heating. However, the ultimate effect on both T and ν is generally minor. The most significant difference between `Low-Ang` and `Soft-Land` is that the latter has a lower accretion rate in a narrow region at the edge of the disk. However, this feature is short lived: It is prominent at 10^2 yr and visible 10^3 yr (Figure 4), but by 10^4 yr (not shown in the figure) there is essentially no difference at all.

3.2. Solid Pileup at the Disk Edge

`DustPy` computes the radial speed of dust particles, taking into account the gas viscous evolution and the inward radial drift of solids relative to the gas

$$v_{r,\text{dust}} = \frac{v_{r,\text{gas}} - 2\eta v_k}{1 + \text{St}^2} \quad (33)$$

$$\eta = -\frac{1}{2} \left(\frac{c_s}{v_k} \right)^2 \frac{\partial \ln P}{\partial \ln r} \quad (34)$$

`DustPy` can optionally include back-reaction, but we did not explore that effect in our model. We estimate that the error in $v_{r,\text{dust}}$ is no more than $\sim 2\%$ for our runs. The green contour of Figure 3 marks the region where dust moves outward ($v_{r,\text{dust}} > 0$).

In a Class II disk $v_{r,\text{gas}}$ is small and often neglected, but in a rapidly expanding disk it can dominate and lead to extended regions where dust flows outward. As distance from the star increases, there is a point where the $2\eta v_k$ term in Equation 33 dominates over $v_{r,\text{gas}}$ and $v_{r,\text{dust}}$ changes sign. Because $v_{r,\text{dust}}$ depends on the grain size, the extent of the region with dust outflow is also grain size dependent. At 10^3 yr all models show a sharp edge where all grains stop their outward flow at nearly the same location. That edge softens as the gas continues to expand viscously, preferentially carrying smaller grains with it.

Figure 5 shows the radial velocity of particles and the dust-to-gas ratio at 10^4 yr. We choose $t = 10^4$ yr because this is the snapshot that most clearly shows that there are two distinct dust pile-ups: one associated with the snowline, and a different one associated with the transition between $v_{r,\text{dust}} > 0$ to $v_{r,\text{dust}} < 0$, at the edge of the expanding disk. At $t = 10^3$ yr the two pileups mostly overlap and are difficult to distinguish, and at

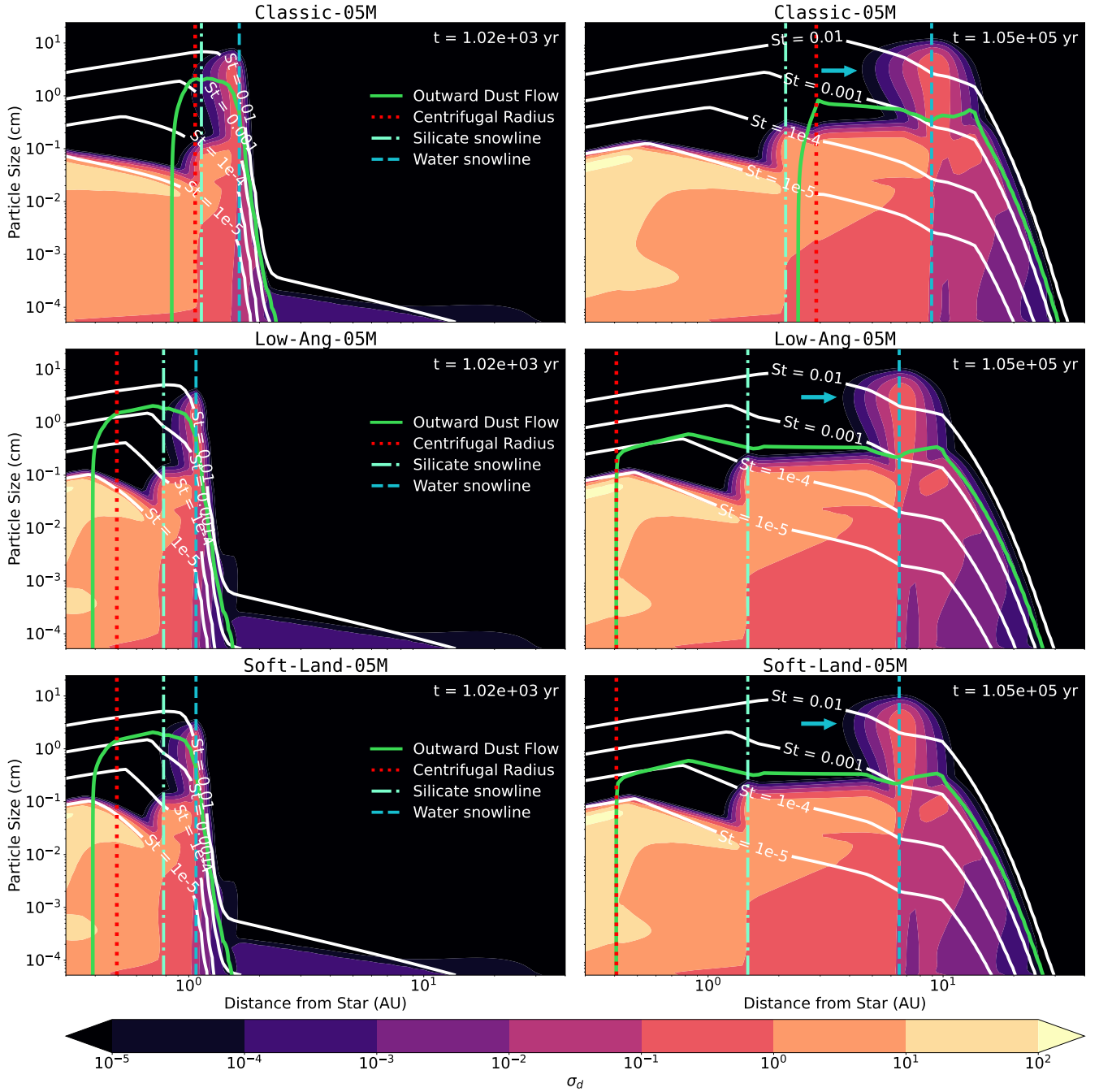


Figure 3. Snapshots of the surface density of dust grains (Σ_d) at 10^3 yr (left) and 10^5 yr (right) for all models with $M_{*,0} = 0.5M_{\odot}$. The green contour marks the range of distances and grain sizes where the net radial velocity of the dust is outward. Infall occurs up to the centrifugal radius (red dotted line). The silicate ($T = 1,000\text{K}$) and water ($T = 170\text{K}$) snowlines are marked as cyan dot-dashed and blue dashed lines, respectively, as well as contours for Stokes numbers $St = 10^{-2}$ and 10^{-3} (white). The blue arrows at 10^5 yr show a feature where small dust grains are advected outward, cross the water snowline, and then drift back inward as they grow in size at the snowline. This loop causes a small increase in surface density at or just interior to the water snowline (see Figure 6).

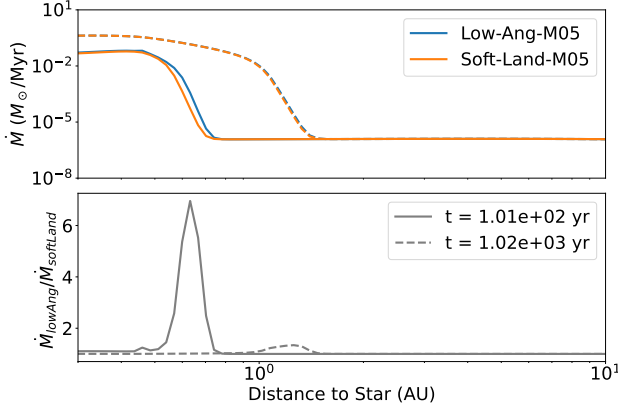


Figure 4. *Top:* Accretion rate (in units of M_{\odot} per Myr) of the Low-Ang-M05 and Soft-Land-M05 models at 10^2 yr and 10^3 yr. *Bottom:* Ratio of their accretion rates. At 10^2 yr there is a significant difference right at the edge of the disk. At 10^3 yr there is a small but detectable difference, again at the edge of the disk. At 10^4 yr (not shown) the accretion rates are indistinguishable

$t = 10^5$ yr the outer pileup has largely dissipated. Furthermore, the bottom of Figure 5 shows that, at 10^4 yr, an inflationary disk can double the dust-to-gas ratio at the outer edge: The typical dust-to-gas ratio across the disk is $Z = 0.01$ but close to the point where $v_{r,\text{dust}}$ changes sign, it reaches $Z = 0.024$, while the pile up just interior to the snowline is small.

Figure 6 shows the surface density of the gas and dust, as well as the dust-to-gas ratio $Z = \Sigma_d/\Sigma_g$ for all three models at 10^3 yr and 10^5 yr. At 10^5 yr, the pile up at the snowline has grown to almost double the initial dust-to-gas ratio, while the pile up at the edge of the disk has disappeared.

3.3. Limited Pileup at Snowlines

The key result of Morbidelli et al. (2022) is that the water and silicate condensation fronts both produce a large pileup of solids that can lead to contemporaneous planetesimal formation at both locations. This is caused by an “advect-grow-drift” cycle in which silicate and water vapor flow outward by advection and diffusion, which promotes grain growth, and then those grains experience radial drift so that they cross the sublimation line once again.

We find no evidence of the “advect-grow-drift” cycle or a solid pile up at the silicate line. While our runs do not explicitly track silicate vapor, our v_{frag} transition at the silicate line should mimic silicate vapor very accurately. In effect, we model silicate vapor as $\text{St} \sim 10^{-5}$ grains, which are nearly perfectly coupled to the gas and experience advection and diffusion just as silicate vapor would. The green contours in Figure 3 show the region

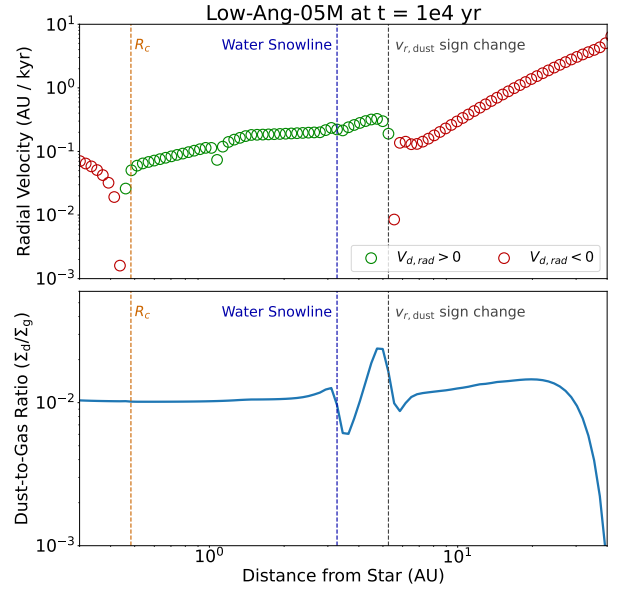


Figure 5. *Top:* Mean (mass-weighted) radial velocity of dust, $v_{r,\text{dust}} = \sum \rho_i v_i / \sum \rho_i$, for the Low-Ang-M05 model at 10^4 yr. The dashed lines show the location of the centrifugal radius R_c , the water snowline, and where $v_{r,\text{dust}}$ changes sign. *Bottom:* Dust-to-gas ratio for the same snapshot. The plot shows two distinct dust pileups: One associated with the water snowline, and another with the change in sign of $v_{r,\text{dust}}$.

where solid grains move outward ($v_{r,\text{dust}} > 0$). Notice that the grains on the far side of the silicate line are still inside the $v_{r,\text{dust}} > 0$ contour. For this reason, the “advect-grow-drift” cycle cannot occur.

For completeness, we looked at every snapshot in our simulations. We did find a brief moment at 0.2 Myr where the Low-Ang-M05 and Soft-Land-M05 models do show larger grains turning around at the silicate line. However, this occurs only for a brief moment, and has no discernible effect on the dust density.

Would our results change if we modeled silicate condensation? We argue that they would not: The grain sizes near the silicate line are limited by the fragmentation barrier. Condensation may increase the grain growth rate, but once grains reach the fragmentation barrier, collisions between grains halts further growth. Therefore, the key finding that silicate grains are too small to drift back in would remain true.

We do find clear evidence of the “advect-grow-drift” cycle at the water snowline, as seen in Figure 3. The green contours mark the region where $v_{r,\text{dust}} > 0$. Across the water snowline, grains grow large enough to exit the green contour. The blue arrows in Figure 3 show the large grains from the water snowline drifting back in. We also see, in Figure 6 (cyan arrows), that just

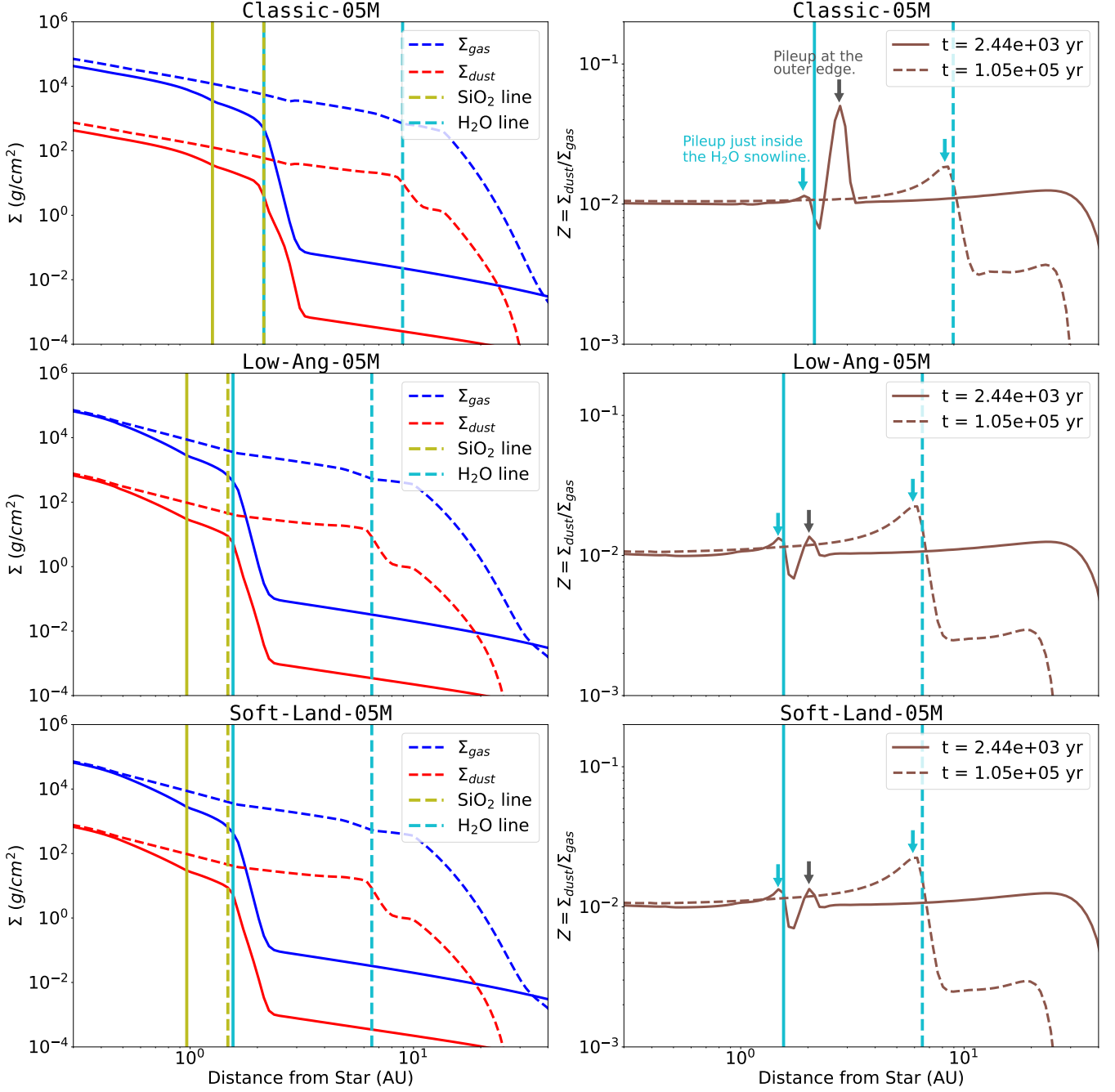


Figure 6. Snapshots of Σ_{gas} and Σ_{dust} at 2.44×10^3 yr and 10^5 yr for all models with an initial stellar mass of $0.5M_{\odot}$. The 2.44×10^3 yr was chosen because it is the earliest snapshot that shows a dust pileup at the outer edge. *Left:* Gas and dust density. *Right:* Dust-to-gas ratio. The silicate ($T = 1,000\text{K}$) and water ($T = 170\text{K}$) snowlines are marked. The blue arrows point to the pileup just interior to the water snowline. The gray arrows point to the pileup associated with the outer edge of the disk, which appears at 2.44×10^3 yr and dissipates by 10^5 yr.

inside the water snowline there is a clear accumulation of solids.

These results are in partial agreement with [Morbidelli et al. \(2022\)](#) in that they also found a “advect-grow-drift” cycle at the water snowline. However, we do not see this behavior at the silicate line, whereas they did. We speculate on the reasons for the differences in Section 4.1

3.4. CAIs and Snowlines

Figure 7 shows the disk temperature profile of the **Classic-M05** and **Low-Ang-M05** models over the entire 1Myr simulation. We do not show **Soft-Land-M05** as it is nearly the same as **Low-Ang-M05**.

In Figure 7 we intentionally remove the outer region where the disk has not yet reached through viscous spreading. For the purpose of these figures, we define the outer edge of the disk as the location where Σ_g has increased in time by a factor of 100 from its initial value $\Sigma_g(t = 0)$ as the disk expands outward. We found this to be a reliable way to identify the exponential drop-off in Σ_g at the outer edge.

One of the most important problems in meteoritics is the formation of Calcium-Aluminum-rich Inclusions (CAIs). Most CAIs formed as fine-grained condensates at very high temperatures ($> 1,300\text{K}$). Figure 7 shows a contour line at $T = 1,400\text{K}$ as a rough estimate of the time and place where CAIs might have condensed. Our results suggest that, regardless of the infall model, CAIs can form in the inner disk, as far out as $\sim 0.5\text{AU}$, throughout the first $\sim 0.3\text{Myr}$ of the disk’s life. This timing remains the same in our ***-M03** models, and is remarkably consistent with what is known of the chronology of CAI formation, which appear to have formed in a $\sim 0.16\text{Myr}$ window ([Connelly et al. 2012](#)). Interestingly, the location the CAI formation line is relatively constant for the first 10^5 years of the **Low-Ang-M05** simulation; unfortunately this is not a testable prediction as CAIs spread over a wide region through advection, drift, and diffusion ([Woitke et al. 2024](#)).

In the last section we noted an increase in the solid-to-gas ratio around the water snowline. Considering that the water snowline may play an important role in planet formation, it is notable that it sweeps through the disk, starting at $\sim 1\text{AU}$ and then reaches as far as $\sim 6\text{AU}$ at around $\sim 0.2\text{Myr}$ before moving back toward the star.

3.5. Grain Sizes and Planetesimal Formation

At each radial location in the disk we computed the mean Stokes number, weighted by mass, St_{mean} , and the Stokes number of the particle mass bin that contains the highest total mass, St_{peak} .

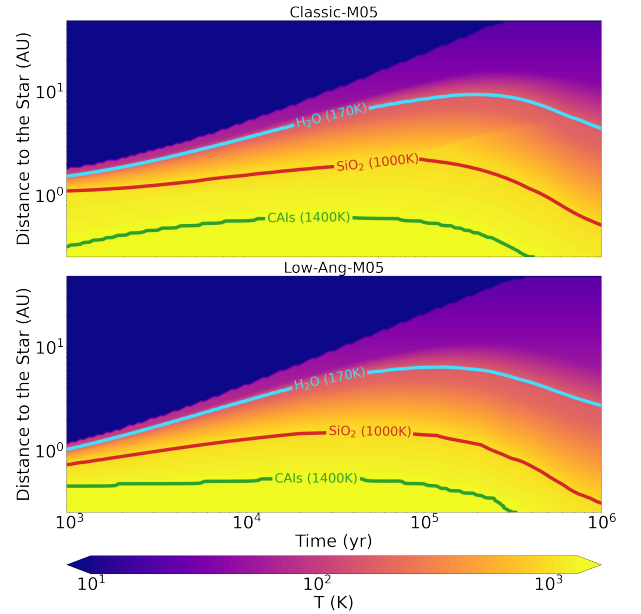


Figure 7. Spacetime diagrams of the disk temperature for the **Classic-M05** and **Low-Ang-M05** models. We also show the water snowline (cyan), the silicate condensation line (red) and the temperature where Ca-Al-rich Inclusions (CAIs) probably condense (green).

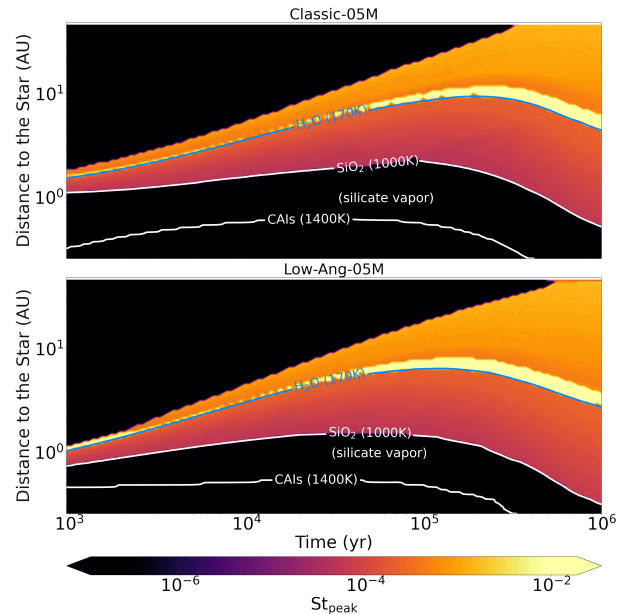


Figure 8. Spacetime diagrams of St_{peak} — the particle Stokes number where most of the mass is concentrated — for the **Classic-M05** and **Low-Ang-M05** models. There are three sharp transitions in particle size, corresponding to the silicate line, the water snowline, and the point at lower temperatures where water ice becomes less sticky ([Musiulik & Wurm 2019](#)).

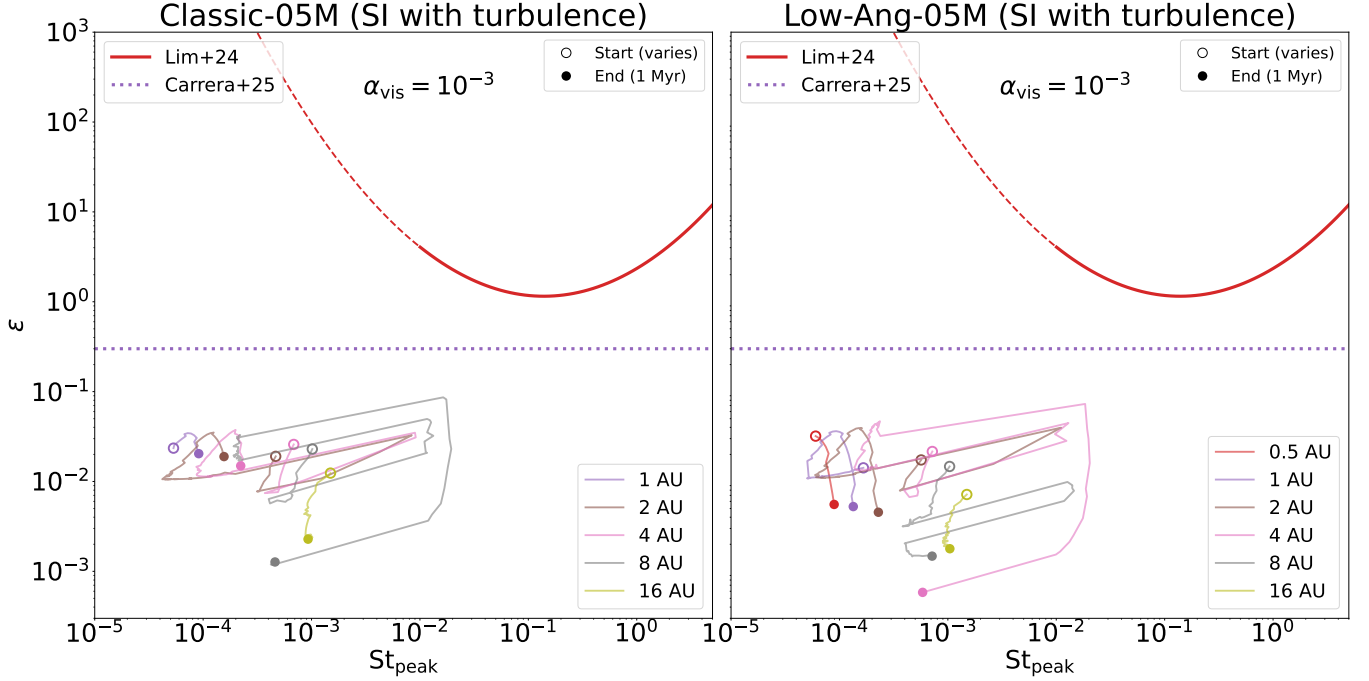


Figure 9. Particle tracks at select locations in the disk for the **Classic-M05** and **Low-Ang-M05** models. The red curve is the SI criterion of [Lim et al. \(2024\)](#), which accounts for how turbulence affects the SI (the dashed line is an extrapolation of their result). The purple dotted line is the threshold of [Carrera et al. \(2025\)](#), where the combination of dust coagulation and turbulence dampening may be able to bring SI filaments into the planetesimal-forming region. We use St_{peak} (Equation 36) as the characteristic Stokes number. The particle tracks start at the time when $T < 1,000\text{K}$ (i.e., when silicates condense) and/or the disk edge reaches that radial location. The key result is that, even accounting for the *concentration-coagulation* feedback loop of [Carrera et al. \(2025\)](#), the conditions of the disk do not allow planetesimal formation via the SI.

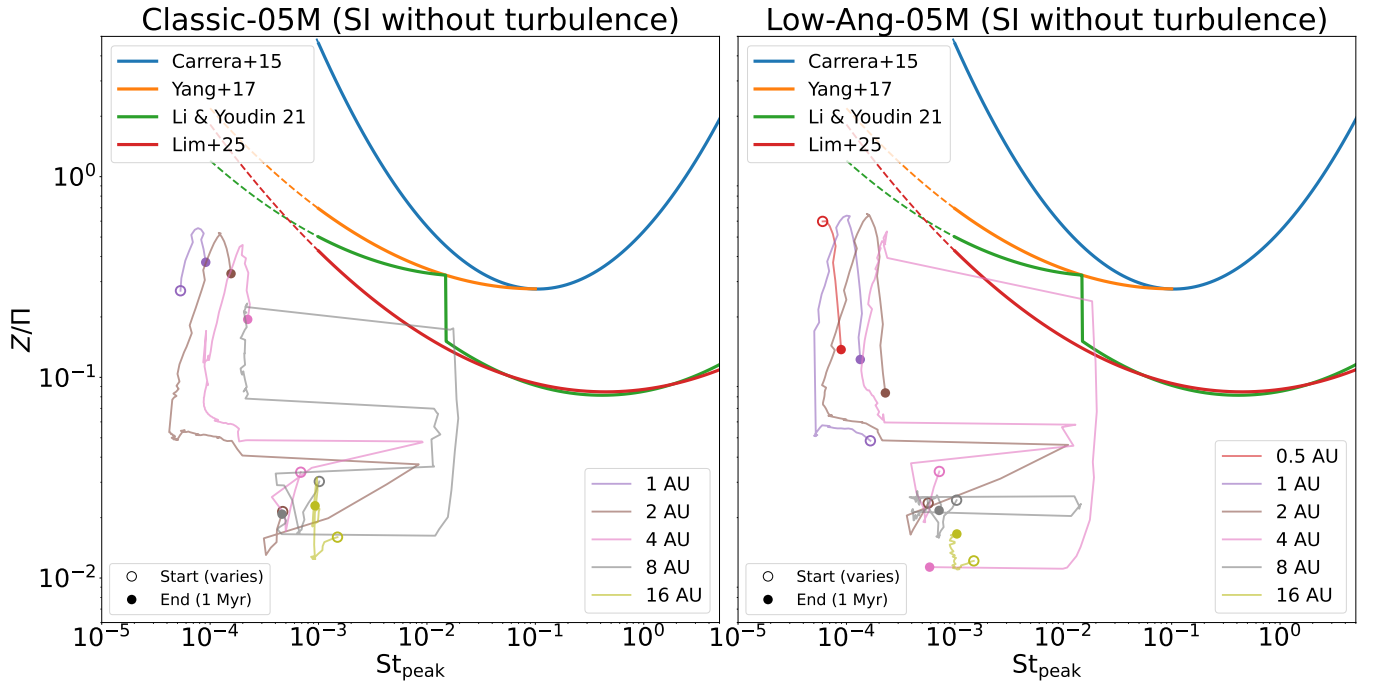


Figure 10. Same as Fig. 9 but showing the SI criteria that do not account for external turbulence ([Lim et al. 2025](#); [Li & Youdin 2021](#); [Yang et al. 2017](#); [Carrera et al. 2015](#)). Note the use of Z/Π on the vertical axis in this figure instead of ϵ . Here Π is a “headwind parameter” that drives SI self-turbulence (for details, see those papers and [Sekiya & Onishi 2018](#)).

$$St_{\text{mean}} = \frac{\sum_i St_i \sigma_i}{\sum_i \sigma_i} \quad (35)$$

$$St_{\text{peak}} = St_i \quad \text{where} \quad i = \text{argmax}(\sigma_i) \quad (36)$$

where St_i is the Stokes number of particles in mass bin i , and σ_i is the mass density in that mass bin.

Figure 8 shows spacetime diagrams of St_{peak} for the **Classic-M05** and **Low-Ang-M05** models. We omit the plots for St_{mean} because they look nearly the same as those of St_{peak} . We also omit the **Soft-Land-M05** model as it is nearly the same as **Low-Ang-M05**. Importantly, we also remove the region interior to the silicate snowline as all silicates are in the form of vapor (strictly speaking there are CAIs, but they have a negligible contribution to the metal content of the disk).

The most prominent feature of Figure 8 is the two sharp changes in particle size. These correspond to the water snowline and the colder point just outside of the snowline where water ice becomes less sticky (Musiolik & Wurm 2019). This creates a relatively narrow band with larger grains.

Figure 9 shows the evolution of the midplane dust-to-gas ratio ϵ and the characteristic grain size St_{peak} at various locations in the disk. The red curve is the SI criterion of Lim et al. (2024) with $\alpha_{\text{vis}} = 10^{-3}$.¹ This is the first study of where in particle size vs. dust-to-gas ratio parameter space SI filaments reach the Roche density in the presence of external turbulence. Here we use the criterion for $\alpha_{\text{vis}} = 10^{-3}$, in line with our simulations. The dashed red line is an extrapolation of the SI criterion beyond the range of the parameters examined by Lim et al. (2024).²

Next, the purple dotted line in Figure 9 is the $\epsilon = 0.3$ threshold obtained by Carrera et al. (2025), who derived a semi-analytic expression to account for the interaction between the SI and dust growth. The key idea behind that work is that SI filaments dampen turbulence due to particle feedback; this promotes grain growth, which in turn makes the SI more effective. They found that, as long as the midplane dust-to-gas ratio can reach $\epsilon = 0.3$, this *concentration-coagulation* feedback loop can bring SI filaments into the planetesimal formation region of Lim et al. (2024). Figure 9 shows that the (ϵ, St) in the disk are at least an order of magnitude away from what

is needed for this concentration-coagulation mechanism to work.

As a side-note, several particle tracks in Figure 9 show a sharp turn to the right (i.e., toward higher St) followed by a decline in ϵ . This happens when the water snowline passes through that location in the disk.

Figure 10 is the same as Figure 9, but instead showing the various SI criteria that do not account for the effect of turbulence on the SI. Comparing these figures shows two things:

- Our results show that, under realistic conditions for a Class 0/I disk, even taking into account both localized dust enhancements at the water snowline or the outer edge of an inflationary disk, as well as the concentration-coagulation feedback loop of Carrera et al. (2025), planetesimal formation via the SI is far out of reach. Even a moderate amount of turbulence ($\alpha_{\text{vis}} = 10^{-3}$) has a significant deleterious effect on the SI. Turbulence decreases the midplane dust concentration and Lim et al. (2024) showed that it also interferes with the SI's ability to form dense particle filament.
- Even the SI criteria that do not account for external turbulence at all (Carrera et al. 2015; Yang et al. 2017; Li & Youdin 2021; Lim et al. 2025) are mostly inconsistent with planetesimal formation in any but a handful of locations.

3.6. Effect of Initial Stellar Mass

Morbidelli et al. (2022) and Marschall & Morbidelli (2023) conducted simulations with $M_{\star} = 0.5M_{\odot}$, so it is important that our first set of simulations followed that example to facilitate comparison. However, as these are very young systems, it is worthwhile exploring smaller initial stellar masses. For example, the stellar mass determines the centrifugal radius, the gravitational potential energy of infall, and the region of the disk where gas or dust flow outward.

Figure 11 shows snapshots of the surface density of grains for the runs with an initial stellar mass of $0.3M_{\odot}$, taken at the same times as those in Figure 3. The figures look quite similar. The biggest differences are seen in the early snapshots ($t = 10^3\text{yr}$) — most notably, the **Classic** model starts out smaller and colder — but by $t = 10^5\text{yr}$ it is somewhat difficult to tell the two sets of simulations apart. There are some differences in the radial extent of the disk and the extent of the region with outward dust flow, but they do not affect the key results in any significant way. The spacetime diagrams all look very similar. In Figure 12 we see that the particle tracks are quite similar to those in Figure 9, including the main

¹ In Lim et al. (2024), the turbulence parameter was simply α . However, it is equivalent to our α_{vis}

² While this is indeed an extrapolation and should be taken with caution, it is clear from the Figure that particle sizes do not even come close to the planetesimal-forming region

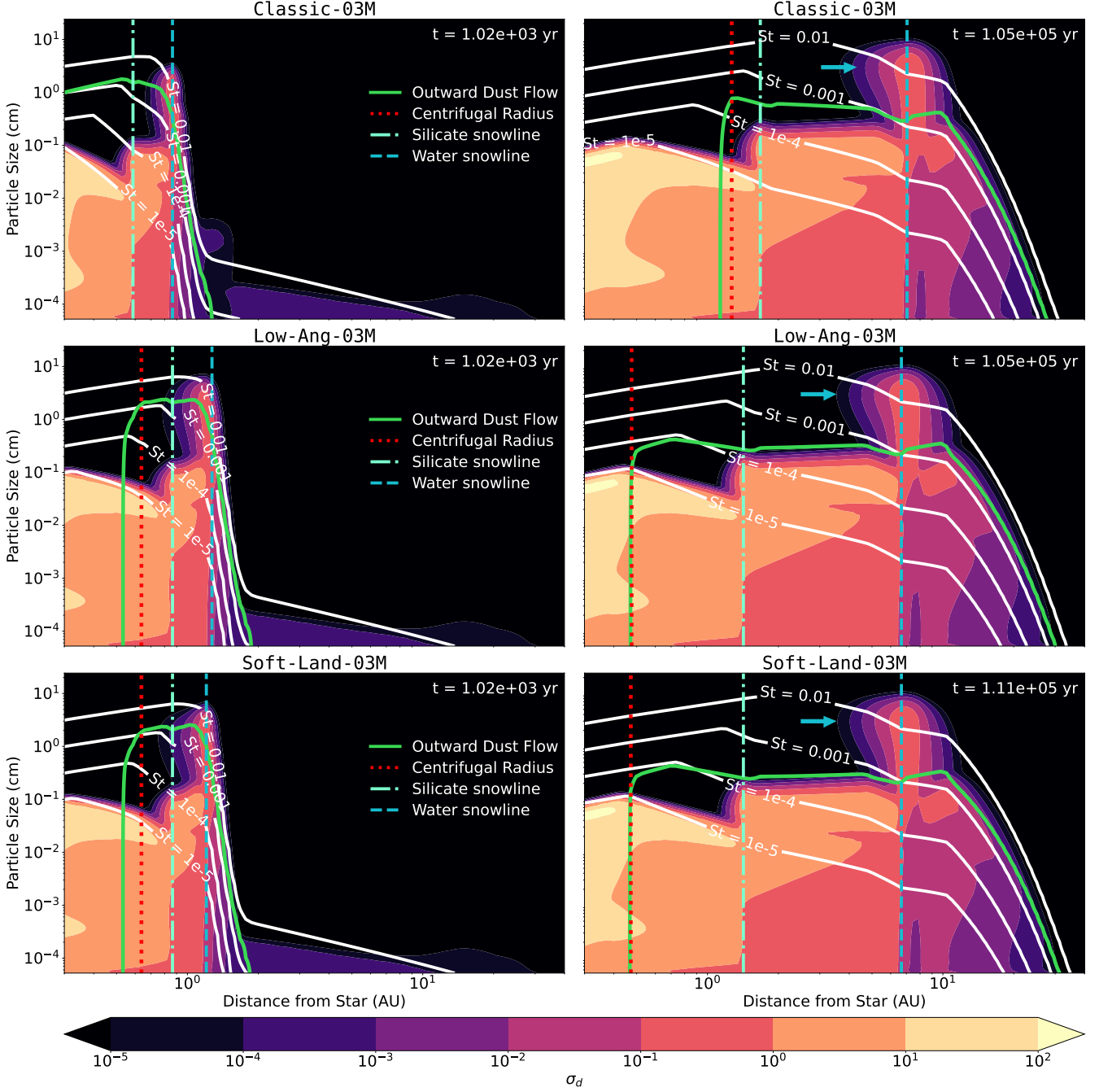


Figure 11. Same as Fig. 3 but with the $M_{*,0} = 0.3M_{\odot}$ models. The results are similar to the ones with $M_{*,0} = 0.5M_{\odot}$. The stellar mass affects the centrifugal radius, which in turn affects the size of the disk and the radial extent of the region with outward dust flow. The **Classic-M03** model is much smaller and colder than **Classic-M05**, while the others become slightly warmer. Aside from that, the changes are generally minor and do not seem to fundamentally change any of the key results.

result that the conditions in the disk are at least an order of magnitude away from what is required to form planetesimals by the SI in a turbulent medium, even considering the criteria for the *concentration-coagulation* feedback loop proposed by [Carrera et al. \(2025\)](#).

4. DISCUSSION

4.1. Comparison with Previous Works

[Estrada & Umurhan \(2023\)](#) conducted an investigation of dust growth in a disk without infall and reached similar conclusions to ours. In particular, their results for $\alpha = 10^{-3}$ are very similar to our particle trajectories for the SI criteria without external turbulence (Figure

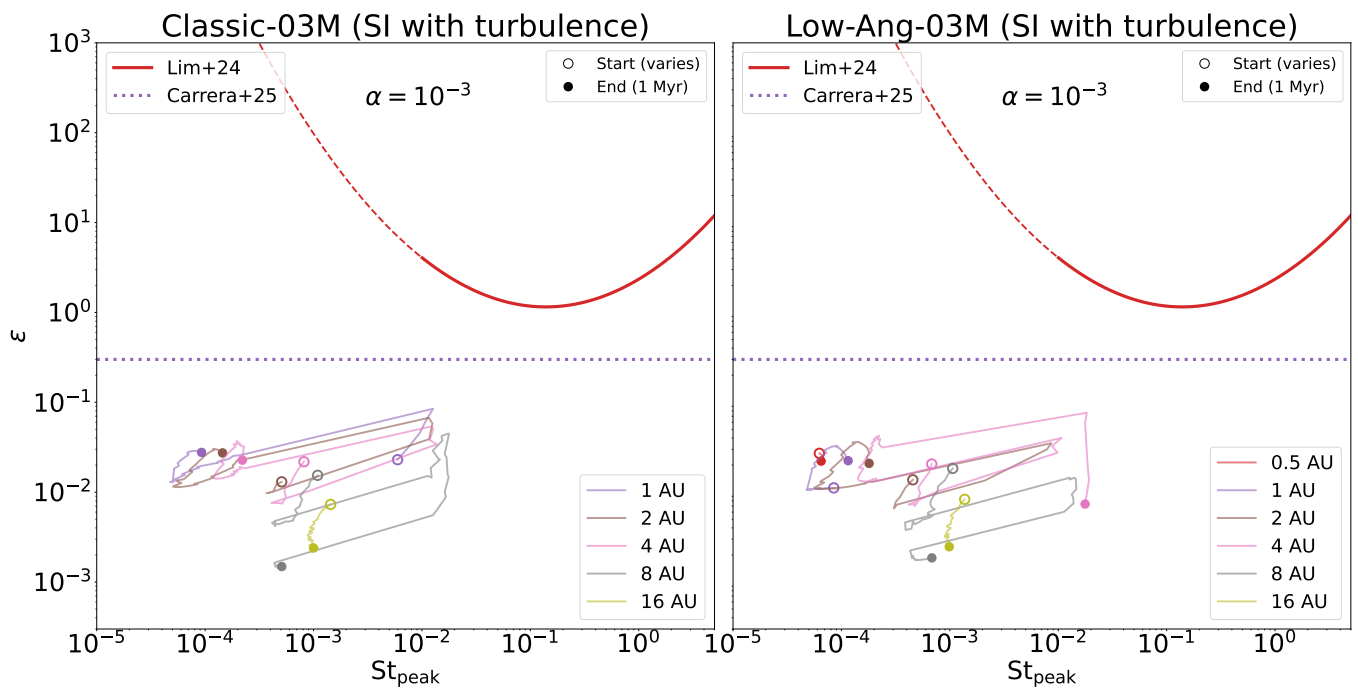


Figure 12. Same as Fig. 9 but for the Classic-M03 and Low-Ang-M03 models.

10).³ One important contribution of their work is that they also explored $\alpha = 10^{-4}$ and found that the larger grains still did not reach the SI criterion. In comparison, our work adds infall and we focus on the more recent works on how the SI criterion is affected by external turbulence.

Additionally, upon finishing this paper, a recent paper came out on the effect of MHD disk winds on the early evolution of Class 0/I disks and the growth of dust grains (Kawasaki & Machida 2025). We discuss this paper more in Section 4.3 when we talk about winds. However, here we point out that while the exact details of their models differ from ours, Kawasaki & Machida (2025) find that assuming both magnetically driven turbulence via the magnetorotational instability (MRI; Balbus & Hawley 1998) and gravitoturbulence (which played a larger role in their simulations due to an increased radial extent of their disk) driving accretion, planetesimal formation is also significantly limited.

Our model and those in Estrada & Umurhan (2023), Morbidelli et al. (2022), and Kawasaki & Machida (2025) all differ in some way.

- Like Estrada & Umurhan (2023) and Kawasaki & Machida (2025), we have a dust evolution model that tracks the entire particle size distribution.
- Like Morbidelli et al. (2022) and Kawasaki & Machida (2025), we model a Class 0/I inflationary disk with infall.
- Unlike our work, all three of these works track vapor species and condensation.

Thus, while we do not fully understand why our results are discrepant with Morbidelli et al. (2022), our hypothesis is that solving for the entire size distribution of particles (as is done with `DustPy` here) is the critical ingredient. However, more work is needed to test this notion, which we leave open for a future investigation.

4.2. Open Questions Related to the α Model

In their seminal work, Shakura & Sunyaev (1973) advanced a physical argument that angular momentum transport caused by magnetic and turbulent stress is proportional to the gas pressure. In this so-called “ α model”, disk viscosity is given by

$$\nu = \alpha \frac{c_s^2}{\Omega} \propto \alpha \frac{T}{\Omega} \quad (37)$$

³ For simplicity of notation, we dropped the “vis” subscript on α in this section

It is also common to choose constant α , which then makes ν linear with T . This is certainly true for our work (except for a negligible contribution from self-gravity) and related works such as Morbidelli et al. (2022); Marschall & Morbidelli (2023); Estrada & Umurhan (2023). Because so many 1D models rely on the α model’s assumption that viscosity is dependent on temperature, it is worth exploring how this assumption might affect our results. For example, a linear dependence T and ν has not been robustly established. Focusing on the magnetorotational instability (MRI; Balbus & Hawley 1998), Sano et al. (2004) and Lyra et al. (2008) both found that the turbulent stress due to the MRI has a power-law dependence on pressure ($\propto P^n$) with an exponent of $n = 0.25$, instead of a linear one. But Minoshima et al. (2015) argued that the exact relation depends on the numerical scheme, and Ross et al. (2016) argued that the small n is an artifact of small simulation domains. Instead, they found that the exponent depends on the magnetic flux and diffusivity, with a range from $n = 0.5$ to 0.9 (close to the α model). Shadmehri et al. (2018) argued that $n < 0.5$ leads to unrealistically steep radial profiles for Σ and T . All this is to say, the exact relationship between ν and T in MRI-driven turbulence is an area of active research, and if it is very different from linear, that could impact our results.

There are other purely hydrodynamic mechanisms that may also contribute to an effective α , namely the Zombie Vortex Instability (ZVI; Marcus et al. 2015), the Convective Overstability (COV; Klahr & Hubbard 2014; Lyra 2014), and the Vertical Shear Instability (VSI; Nelson et al. 2013).⁴

While these hydrodynamic mechanisms are intimately linked to the thermal properties of the gas (e.g., the cooling timescale controls which mechanism dominates), to our knowledge, the only detailed study of the temperature dependence of turbulent stresses from these hydrodynamic mechanisms is a focus on the VSI by Manger et al. (2021). They found that the stress induced by the VSI scales not with the pressure but instead with the square of the exponent of the radial temperature profile (for a limited range of exponent values). Thus, as with the MRI studies, the relationship between ν and T from purely hydrodynamic mechanisms remains somewhat unclear.

4.3. Disk Winds

⁴ We don’t include a discussion of gravitoturbulence within the context of the α model here since it plays a negligible role in our calculations.

Perhaps the most important missing ingredient in our model is disk winds. Starting with the concept of α viscosity from [Shakura & Sunyaev \(1973\)](#), one can write α as the density-weighted Maxwell and Reynolds $r\phi$ component to the stress tensor ([Balbus & Hawley 1998](#))

$$W_{r\phi} \equiv \frac{\langle \rho v_r \delta v_\phi - B_r B_\phi \rangle}{\langle \rho c_s^2 \rangle} \quad (38)$$

$$\alpha \equiv \overline{|W_{r\phi}|} \quad (39)$$

where ϕ is the azimuthal direction, δv_ϕ is the azimuthal velocity with Keplerian shear subtracted, and \mathbf{B} is the magnetic field. In a steady-state disk where $W_{r\phi}$ is the only source of accretion, the accretion rate is given by

$$\dot{M}_{R\phi} = \frac{2\pi c_s^2 \Sigma}{\Omega} \alpha \quad (40)$$

Conversely, the accretion rate for a steady-state disk where the only source of accretion is a disk wind is defined via the $z\phi$ component of the stress tensor, $W_{z\phi}$ (see [Simon et al. 2013](#)) as

$$\dot{M}_{z\phi} = \frac{8rc_s^2 \Sigma}{H\Omega} |W_{z\phi}| \sqrt{\frac{\pi}{2}} \quad (41)$$

$$W_{z\phi} \equiv \frac{\rho v_z \delta v_\phi - B_z B_\phi}{\rho_0 c_s^2} \Big|_{-z_{\text{bw}}}^{z_{\text{bw}}} \quad (42)$$

where $\pm z_{\text{bw}}$ are integration limits corresponding to the base of the wind on either side of the disk (see [Simon et al. 2013](#), for details). Note that Equation 41 differs from the expression in [Simon et al. \(2013\)](#) by a factor of $\sqrt{2}$ because they define H differently than we do.

With these ingredients, an approximate expression for the accretion rate in a disk with both viscous stress and disk winds is

$$\dot{M} = \frac{2\pi c_s^2 \Sigma}{\Omega} \left[\alpha + \sqrt{\frac{8}{\pi}} \frac{r}{H} |W_{z\phi}| \right]. \quad (43)$$

Finally, [Simon et al. \(2013\)](#) estimate that $|W_{z\phi}|$ is in the same magnitude range as α . If so, given that $r/H \gg 1$, disk winds may be the dominant driver of accretion, even in the Class 0/I stage. There are a few ways that our results might change under wind-dominated accretion:

1. Less viscous spreading.

Winds contribute to accretion, but not to viscous spreading. A wind-dominated disk would spread less, which would reduce the amount of solid material advected across snowlines. This may pose an additional challenge for the SI. That said, even a wind-dominated disk could have significant

spreading in the early GI-dominated phase. If so, the SI might be active only in these early stages.

2. Less heating.

By the same token, lower viscosity for a given \dot{M} would make the disk colder. In our models viscous heating is the dominant source of heat in the inner disk. Removing a significant fraction of that would bring the silicate and water snowlines much closer to the star. However, St_{frag} at the snowline would remain the same unless α is different (see the next point). Therefore, the implications for the SI are unclear.

3. Lower α ?

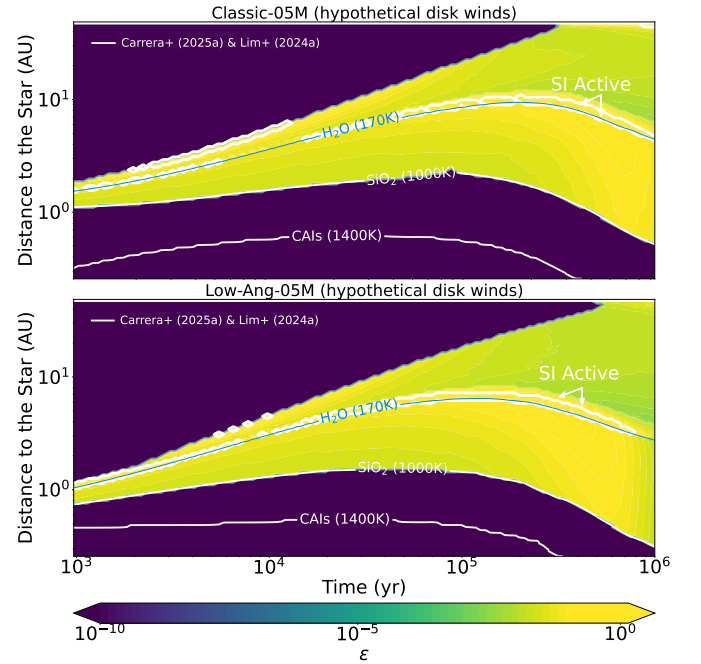


Figure 13. Toy model where we increase St and ϵ by $\times 10$ (equivalent to decreasing α_{vis} to 10^{-4}) but otherwise keep the disk structure intact. There are small regions, mainly around the water snowline and at the outer edge of the disk (though only for the first $\sim 10^4$ yr at the outer edge), where this model reaches the $\epsilon = 0.3$ threshold of [Carrera et al. \(2025\)](#). That is the threshold where their “concentration-coagulation” feedback loop can reach the SI criterion in the presence of turbulence.

For any given disk lifetime or accretion rate \dot{M} , a disk with winds ($W_{z\phi}$) must have a lower α . Note that disk lifetimes and accretion rates are not fully constrained, but a lower α would result in both larger St and greater midplane concentration ϵ .

Since $\text{St}_{\text{frag}} \propto 1/\alpha$ and $\epsilon \propto \sqrt{\text{St}/\alpha} \propto 1/\alpha$, all other things being equal, reducing α_{vis} to 10^{-4}

would increase both (St, ϵ) by a factor of 10. As a proof of concept, we can consider a toy model (Figure 13) where we do just that, but otherwise leave our disk structure intact.

We find that in a wind-dominated disk, planetesimals may form around the water snowline and at the outer edge of the disk (though here, this only lasts for the first $\sim 10^4$ yr). However, the formation region does appear to be limited to these locations.

A couple of caveats with this toy model: Disk winds will surely alter the disk structure, and turbulence is not the only source of grain collisions — for large grains, drift-induced velocities can dominate the collision speed (see the `DustPy` documentation).

However, despite its limitations, this thought experiment can give us some sense of how much disk winds might alter our results.

As mentioned previously, upon writing of this manuscript, [Kawasaki & Machida \(2025\)](#) published a study of dust growth in a Class 0/I disk both with and without MHD winds. Indeed, they found that planetesimal formation via the SI should be significantly easier *with* an MHD wind than without. However, their equivalent of our Figs. 10 and 12 (figures 16 and 17 in their paper) did not include the stricter SI criterion in the presence of turbulence (found by [Lim et al. 2024](#)) even with an MHD wind. While MHD winds may very well dominate angular momentum transport, recent studies (e.g., [Cui & Bai 2021](#); [Rea et al. 2024](#)) have shown that turbulence can persist even when winds play an important role.

While we intend to include winds in a follow up study to investigate this further, these considerations do suggest that planetesimal formation via the SI may still be difficult in Class 0/I disks even if MHD winds dominate the evolution.

4.4. Snowlines

`DustPy` only allows a fairly simplified treatment of the water and silicate snowlines. In a realistic disk, solid material that drifts inward across one of the snowlines will evaporate and join the gas component. Since the gas accretion rate is much slower than solid drift, the evaporated material cannot be removed as quickly in its vapor form as it is supplied in solid form (e.g., [Cuzzi & Zahnle 2004](#)). This is not something that one can currently model with `DustPy`. However, we can speculate on how this concentration of vapor might affect our results:

- One possibility (seen in [Morbidelli et al. 2022](#)), is that vapor could spread back through the snowline. This can increase the total solid mass near the snowline, but it does not necessarily alter grain sizes.
- A second possibility is that vapor condensation might produce larger grains beyond the snowline (e.g., [Ros et al. 2019](#)). However, it is unlikely that the grains would be much larger than the ones in our models because the grain sizes in those models are fragmentation-limited ([Stammler et al. 2017](#)).
- Importantly, [Estrada & Umurhan \(2023\)](#) do track multi-species vapor and condensation, and their results resemble ours.
- Finally, the accumulation of vapor inside the snowline leads to an increase in mean molecular weight, which lowers the sound speed, which leads to the formation of a pressure bump (e.g., [Charnoz et al. 2021](#); [Drazkowska & Dullemond 2018](#); [Drazkowska & Alibert 2017](#)). However, this might not necessarily allow the SI to form planetesimals. [Carrera & Simon \(2022\)](#) conducted a large high-res simulation of the SI with a pressure bump with a particle Stokes number comparable to the ones in these simulations. They found that there was no indication of the SI. However, a sufficiently large pressure bump will form a particle trap and could form planetesimals by gravitational instability (i.e., if enough particles pile up, the local density will surpass the Roche density.)

4.5. Accretion Model

As noted earlier in this paper, the simulations of [Mauxion et al. \(2024\)](#) show a more complex infall geometry than what we use in our model. In particular, the simulations by [Mauxion et al. \(2024\)](#) show that some of the infalling gas occurs along the mid-plane of the disk and shocks the edge of the disk, whereas the remaining infalling gas gently lands on the disk surface. This is at odds with 1D models like ours and those of [Morbidelli et al. \(2022\)](#) and [Marschall & Morbidelli \(2023\)](#) that insert material at the centrifugal radius without considering this more complex geometry. If infall occurs as it does in those simulations, then at least some of the gas is deposited wherever it encounters the edge of the disk, which will influence where shock heating occurs.

In addition, the simulations of [Mauxion et al. \(2024\)](#) show a great deal of structure that is not captured by our current models and may be important for trapping particles. Furthermore, other MHD simulations (even

without infall) also show disk substructures (e.g., zonal flows; Béthune et al. 2017; Hu et al. 2019). We leave the investigation of substructures in Class 0/I disks for future investigations.

5. SUMMARY AND CONCLUSIONS

In this work, we studied the growth of small dust grains into larger particles in a viscously expanding “inflationary” disk and whether or not conditions can be met for the SI to work. Similar to other works, we find that the outward flow of gas counteracts the tendency of solid grains to drift toward the star, resulting in higher concentrations and larger grains. This is most evident at the water snowline, where an “advection-condensation-drift” loop leads to a significant solid pile up. However, we do not see a similar process at the silicate condensation line. Instead, we find that silicate grains just beyond the silicate condensation front are advected outward along with the gas. We do, however, find an additional solid pile up at the edge of the expanding disk that appears to not have been previously reported.

Our investigation stands out from other works in that we explore the implications of recent results on how the SI responds to turbulence. Specifically, Lim et al. (2024) conducted 3D simulations of the SI in the presence of turbulence and Carrera et al. (2025) derived analytic expressions for how the SI interacts with dust coagulation in a turbulent medium. Applying these developments to our disk model, we find that for modest $\alpha_{\text{vis}} = 10^{-3}$ turbulence, the planetesimal formation region is completely out of reach. The midplane dust-to-gas ratio is at least an order of magnitude too small to form planetesimals, even if the SI is assisted by its feedback loop with dust coagulation. Furthermore, the maximum grain size in our simulations remains quite small due to turbulent fragmentation.

All in all, the quest for a formation scenario in which realistic disk conditions are able to satisfy the conditions

for the SI (Carrera et al. 2015; Yang et al. 2017; Li & Youdin 2021; Lim et al. 2025), continues. We still believe that Class 0/I disks and infall deserve careful attention, given the observational evidence that planets form early. An inflationary disk’s ability to overcome the radial drift barrier is promising, but planetesimal formation via the SI appears to be thwarted by disk turbulence, which simultaneously keeps solid grains small and reduces the midplane dust-to-gas ratio. Future works should consider variations of this formation scenario that ideally have less turbulence, or perhaps exploring alternatives to the SI.

As discussed above, one promising route towards early planetesimal formation is magnetic wind-driven accretion, which (for a given accretion rate) implies a small α_{vis} . A simple toy model where we allow grain sizes to grow due to reduced turbulent fragmentation does imply that planetesimal formation is possible in such a disk. However, the regions where this occurs are limited, and there are many simplifications of our toy model that may not hold true when a more self-consistent model is used.

Clearly, planetesimal formation occurs at some point. However, when and how this happens remains debated. Our results imply that planetesimal formation (at least via the SI) may be difficult unless some mechanism keeps turbulence low, and even then, the SI might be limited to the water snowline or other disk structures.

ACKNOWLEDGMENTS

The authors thank Eric Gaidos, Wenrui Xu, Geoffroy Lesur, Tom Megeath, Kaitlin Kratter, and Lee Hartmann for their insightful comments and questions that greatly improved the quality of this work. DC and JBS acknowledge support from NASA under *Emerging Worlds* through grant 80NSSC21K0037, and *Exoplanets Research* through grants 80NSSC24K0959 and 80NSSC22K0267. CH acknowledges support from the National Science Foundation through NSF AAG grant No.8612407679.

REFERENCES

- Balbus, S. A., & Hawley, J. F. 1998, *Reviews of Modern Physics*, 70, 1, doi: [10.1103/RevModPhys.70.1](https://doi.org/10.1103/RevModPhys.70.1)
- Bell, K. R., & Lin, D. N. C. 1994, *ApJ*, 427, 987, doi: [10.1086/174206](https://doi.org/10.1086/174206)
- Béthune, W., Latter, H., & Kley, W. 2021, *A&A*, 650, A49, doi: [10.1051/0004-6361/202040094](https://doi.org/10.1051/0004-6361/202040094)
- Béthune, W., Lesur, G., & Ferreira, J. 2017, *Astronomy & Astrophysics*, 600, A75, doi: [10.1051/0004-6361/201630056](https://doi.org/10.1051/0004-6361/201630056)
- Birnstiel, T., Dullemond, C. P., & Brauer, F. 2010, *A&A*, 513, A79, doi: [10.1051/0004-6361/200913731](https://doi.org/10.1051/0004-6361/200913731)
- Birnstiel, T., Klahr, H., & Ercolano, B. 2012, *A&A*, 539, A148, doi: [10.1051/0004-6361/201118136](https://doi.org/10.1051/0004-6361/201118136)
- Bitsch, B., Crida, A., Morbidelli, A., Kley, W., & Dobbs-Dixon, I. 2013, *A&A*, 549, A124, doi: [10.1051/0004-6361/201220159](https://doi.org/10.1051/0004-6361/201220159)
- Blum, J., & Wurm, G. 2008, *ARA&A*, 46, 21, doi: [10.1146/annurev.astro.46.060407.145152](https://doi.org/10.1146/annurev.astro.46.060407.145152)

- Carrera, D., Gorti, U., Johansen, A., & Davies, M. B. 2017, *ApJ*, 839, 16, doi: [10.3847/1538-4357/aa6932](https://doi.org/10.3847/1538-4357/aa6932)
- Carrera, D., Johansen, A., & Davies, M. B. 2015, *A&A*, 579, A43, doi: [10.1051/0004-6361/201425120](https://doi.org/10.1051/0004-6361/201425120)
- Carrera, D., Lim, J., Eriksson, L. E. J., Lyra, W., & Simon, J. B. 2025, arXiv e-prints, arXiv:2503.03105, doi: [10.48550/arXiv.2503.03105](https://doi.org/10.48550/arXiv.2503.03105)
- Carrera, D., & Simon, J. B. 2022, *ApJL*, 933, L10, doi: [10.3847/2041-8213/ac6b3e](https://doi.org/10.3847/2041-8213/ac6b3e)
- Carrera, D., Simon, J. B., Li, R., Kretke, K. A., & Klahr, H. 2021, *AJ*, 161, 96, doi: [10.3847/1538-3881/abd4d9](https://doi.org/10.3847/1538-3881/abd4d9)
- Chambers, J. E. 2001, *Icarus*, 152, 205, doi: [10.1006/icar.2001.6639](https://doi.org/10.1006/icar.2001.6639)
- Charnoz, S., Avicé, G., Hyodo, R., Pignatale, F. C., & Chaussidon, M. 2021, *A&A*, 652, A35, doi: [10.1051/0004-6361/202038797](https://doi.org/10.1051/0004-6361/202038797)
- Connelly, J. N., Bizzarro, M., Krot, A. N., et al. 2012, *Science*, 338, 651, doi: [10.1126/science.1226919](https://doi.org/10.1126/science.1226919)
- Cossins, P., Lodato, G., & Clarke, C. 2010, *MNRAS*, 401, 2587, doi: [10.1111/j.1365-2966.2009.15835.x](https://doi.org/10.1111/j.1365-2966.2009.15835.x)
- Cossins, P., Lodato, G., & Clarke, C. J. 2009, *MNRAS*, 393, 1157, doi: [10.1111/j.1365-2966.2008.14275.x](https://doi.org/10.1111/j.1365-2966.2008.14275.x)
- Cui, C., & Bai, X.-N. 2021, *MNRAS*, 507, 1106, doi: [10.1093/mnras/stab2220](https://doi.org/10.1093/mnras/stab2220)
- Cuzzi, J. N., Hogan, R. C., & Shariff, K. 2008, *ApJ*, 687, 1432, doi: [10.1086/591239](https://doi.org/10.1086/591239)
- Cuzzi, J. N., & Zahnle, K. J. 2004, *ApJ*, 614, 490, doi: [10.1086/423611](https://doi.org/10.1086/423611)
- Desch, S. J., Kalyaan, A., & O'D. Alexander, C. M. 2018, *ApJS*, 238, 11, doi: [10.3847/1538-4365/aad95f](https://doi.org/10.3847/1538-4365/aad95f)
- Drazkowska, J., & Alibert, Y. 2017, *A&A*, 608, A92, doi: [10.1051/0004-6361/201731491](https://doi.org/10.1051/0004-6361/201731491)
- Drazkowska, J., & Dullemond, C. P. 2018, *A&A*, 614, A62, doi: [10.1051/0004-6361/201732221](https://doi.org/10.1051/0004-6361/201732221)
- Durisen, R. H., Boss, A. P., Mayer, L., et al. 2007, in *Protostars and Planets V*, ed. B. Reipurth, D. Jewitt, & K. Keil, 607, doi: [10.48550/arXiv.astro-ph/0603179](https://doi.org/10.48550/arXiv.astro-ph/0603179)
- Estrada, P. R., & Umurhan, O. M. 2023, *ApJ*, 946, 15, doi: [10.3847/1538-4357/acb7db](https://doi.org/10.3847/1538-4357/acb7db)
- Fraser, W. C., Bannister, M. T., Pike, R. E., et al. 2017, *Nature Astronomy*, 1, 0088, doi: [10.1038/s41550-017-0088](https://doi.org/10.1038/s41550-017-0088)
- Gammie, C. F. 2001, *ApJ*, 553, 174, doi: [10.1086/320631](https://doi.org/10.1086/320631)
- Goldreich, P., & Lynden-Bell, D. 1965, *MNRAS*, 130, 125, doi: [10.1093/mnras/130.2.125](https://doi.org/10.1093/mnras/130.2.125)
- Gundlach, B., & Blum, J. 2015, *ApJ*, 798, 34, doi: [10.1088/0004-637X/798/1/34](https://doi.org/10.1088/0004-637X/798/1/34)
- Hu, X., Zhu, Z., Okuzumi, S., et al. 2019, *The Astrophysical Journal*, 885, 36, doi: [10.3847/1538-4357/ab44cb](https://doi.org/10.3847/1538-4357/ab44cb)
- Johansen, A., Oishi, J. S., Mac Low, M.-M., et al. 2007, *Nature*, 448, 1022, doi: [10.1038/nature06086](https://doi.org/10.1038/nature06086)
- Johansen, A., & Youdin, A. 2007, *ApJ*, 662, 627, doi: [10.1086/516730](https://doi.org/10.1086/516730)
- Kawasaki, Y., & Machida, M. N. 2025, arXiv e-prints, arXiv:2503.19219, doi: [10.48550/arXiv.2503.19219](https://doi.org/10.48550/arXiv.2503.19219)
- Klahr, H., & Hubbard, A. 2014, *The Astrophysical Journal*, 788, 21, doi: [10.1088/0004-637X/788/1/21](https://doi.org/10.1088/0004-637X/788/1/21)
- Kokubo, E., & Ida, S. 1996, *Icarus*, 123, 180, doi: [10.1006/icar.1996.0148](https://doi.org/10.1006/icar.1996.0148)
- . 2000, *Icarus*, 143, 15, doi: [10.1006/icar.1999.6237](https://doi.org/10.1006/icar.1999.6237)
- Kratter, K., & Lodato, G. 2016, *ARA&A*, 54, 271, doi: [10.1146/annurev-astro-081915-023307](https://doi.org/10.1146/annurev-astro-081915-023307)
- Kruijjer, T. S., Burkhardt, C., Budde, G., & Kleine, T. 2017, *Proceedings of the National Academy of Science*, 114, 6712, doi: [10.1073/pnas.1704461114](https://doi.org/10.1073/pnas.1704461114)
- Lau, T. C. H., Drazkowska, J., Stammler, S. M., Birnstiel, T., & Dullemond, C. P. 2022, *A&A*, 668, A170, doi: [10.1051/0004-6361/202244864](https://doi.org/10.1051/0004-6361/202244864)
- Laughlin, G., & Bodenheimer, P. 1994, *ApJ*, 436, 335, doi: [10.1086/174909](https://doi.org/10.1086/174909)
- Li, R., & Youdin, A. N. 2021, *ApJ*, 919, 107, doi: [10.3847/1538-4357/ac0e9f](https://doi.org/10.3847/1538-4357/ac0e9f)
- Lim, J., Simon, J. B., Li, R., et al. 2025, *ApJ*, 981, 160, doi: [10.3847/1538-4357/adb311](https://doi.org/10.3847/1538-4357/adb311)
- . 2024, *ApJ*, 969, 130, doi: [10.3847/1538-4357/ad47a2](https://doi.org/10.3847/1538-4357/ad47a2)
- Lin, D. N. C., & Pringle, J. E. 1987, *MNRAS*, 225, 607, doi: [10.1093/mnras/225.3.607](https://doi.org/10.1093/mnras/225.3.607)
- Liu, Y., Roussel, H., Linz, H., et al. 2024, arXiv e-prints, arXiv:2411.00277, doi: [10.48550/arXiv.2411.00277](https://doi.org/10.48550/arXiv.2411.00277)
- Lodato, G., & Rice, W. K. M. 2005, *MNRAS*, 358, 1489, doi: [10.1111/j.1365-2966.2005.08875.x](https://doi.org/10.1111/j.1365-2966.2005.08875.x)
- Lynden-Bell, D., & Pringle, J. E. 1974, *MNRAS*, 168, 603, doi: [10.1093/mnras/168.3.603](https://doi.org/10.1093/mnras/168.3.603)
- Lyra, W. 2014, *The Astrophysical Journal*, 789, 77, doi: [10.1088/0004-637X/789/1/77](https://doi.org/10.1088/0004-637X/789/1/77)
- Lyra, W., Johansen, A., Klahr, H., & Piskunov, N. 2008, *A&A*, 479, 883, doi: [10.1051/0004-6361:20077948](https://doi.org/10.1051/0004-6361:20077948)
- Manara, C. F., Morbidelli, A., & Guillot, T. 2018, *A&A*, 618, L3, doi: [10.1051/0004-6361/201834076](https://doi.org/10.1051/0004-6361/201834076)
- Manger, N., Pfeil, T., & Klahr, H. 2021, *MNRAS*, 508, 5402, doi: [10.1093/mnras/stab2599](https://doi.org/10.1093/mnras/stab2599)
- Marcus, P. S., Pei, S., Jiang, C.-H., et al. 2015, *The Astrophysical Journal*, 808, 87, doi: [10.1088/0004-637X/808/1/87](https://doi.org/10.1088/0004-637X/808/1/87)
- Marschall, R., & Morbidelli, A. 2023, *A&A*, 677, A136, doi: [10.1051/0004-6361/202346616](https://doi.org/10.1051/0004-6361/202346616)
- Mathis, J. S., Rumpl, W., & Nordsieck, K. H. 1977, *ApJ*, 217, 425, doi: [10.1086/155591](https://doi.org/10.1086/155591)
- Mauxion, J., Lesur, G., & Maret, S. 2024, *A&A*, 686, A253, doi: [10.1051/0004-6361/202348405](https://doi.org/10.1051/0004-6361/202348405)

- Minoshima, T., Hirose, S., & Sano, T. 2015, *ApJ*, 808, 54, doi: [10.1088/0004-637X/808/1/54](https://doi.org/10.1088/0004-637X/808/1/54)
- Morbidelli, A., Baillié, K., Batygin, K., et al. 2022, *Nature Astronomy*, 6, 72, doi: [10.1038/s41550-021-01517-7](https://doi.org/10.1038/s41550-021-01517-7)
- Morbidelli, A., Bottke, W. F., Nesvorný, D., & Levison, H. F. 2009, *Icarus*, 204, 558, doi: [10.1016/j.icarus.2009.07.011](https://doi.org/10.1016/j.icarus.2009.07.011)
- Morbidelli, A., Chambers, J., Lunine, J. I., et al. 2000, *M&PS*, 35, 1309, doi: [10.1111/j.1945-5100.2000.tb01518.x](https://doi.org/10.1111/j.1945-5100.2000.tb01518.x)
- Mulders, G. D., Pascucci, I., Ciesla, F. J., & Fernandes, R. B. 2021, *ApJ*, 920, 66, doi: [10.3847/1538-4357/ac178e](https://doi.org/10.3847/1538-4357/ac178e)
- Musiolik, G. 2021, *MNRAS*, 506, 5153, doi: [10.1093/mnras/stab1963](https://doi.org/10.1093/mnras/stab1963)
- Musiolik, G., & Wurm, G. 2019, *ApJ*, 873, 58, doi: [10.3847/1538-4357/ab0428](https://doi.org/10.3847/1538-4357/ab0428)
- Nelson, R. P., Gressel, O., & Umurhan, O. M. 2013, *Monthly Notices of the Royal Astronomical Society*, 435, 2610, doi: [10.1093/mnras/stt1475](https://doi.org/10.1093/mnras/stt1475)
- Nesvorný, D., Li, R., Simon, J. B., et al. 2021, *The Planetary Science Journal*, 2, 27, doi: [10.3847/PSJ/abd858](https://doi.org/10.3847/PSJ/abd858)
- Nesvorný, D., Li, R., Youdin, A. N., Simon, J. B., & Grundy, W. M. 2019, *Nature Astronomy*, 3, 808, doi: [10.1038/s41550-019-0806-z](https://doi.org/10.1038/s41550-019-0806-z)
- Nesvorný, D., Youdin, A. N., & Richardson, D. C. 2010, *AJ*, 140, 785, doi: [10.1088/0004-6256/140/3/785](https://doi.org/10.1088/0004-6256/140/3/785)
- Öberg, K. I., & Wordsworth, R. 2019, *AJ*, 158, 194, doi: [10.3847/1538-3881/ab46a8](https://doi.org/10.3847/1538-3881/ab46a8)
- Ormel, C. W., & Cuzzi, J. N. 2007, *A&A*, 466, 413, doi: [10.1051/0004-6361/20066899](https://doi.org/10.1051/0004-6361/20066899)
- Paardekooper, S.-J., Baruteau, C., & Meru, F. 2011, *MNRAS*, 416, L65, doi: [10.1111/j.1745-3933.2011.01099.x](https://doi.org/10.1111/j.1745-3933.2011.01099.x)
- Poppe, T., Blum, J., & Henning, T. 2000, *ApJ*, 533, 454, doi: [10.1086/308626](https://doi.org/10.1086/308626)
- Rafikov, R. R. 2015, *ApJ*, 804, 62, doi: [10.1088/0004-637X/804/1/62](https://doi.org/10.1088/0004-637X/804/1/62)
- Rea, D. G., Simon, J. B., Carrera, D., et al. 2024, *ApJ*, 972, 128, doi: [10.3847/1538-4357/ad57c5](https://doi.org/10.3847/1538-4357/ad57c5)
- Rice, K. 2016, *PASA*, 33, e012, doi: [10.1017/pasa.2016.12](https://doi.org/10.1017/pasa.2016.12)
- Rice, W. K. M., Lodato, G., Pringle, J. E., Armitage, P. J., & Bonnell, I. A. 2004, *MNRAS*, 355, 543, doi: [10.1111/j.1365-2966.2004.08339.x](https://doi.org/10.1111/j.1365-2966.2004.08339.x)
- Ros, K., Johansen, A., Riipinen, I., & Schlesinger, D. 2019, *A&A*, 629, A65, doi: [10.1051/0004-6361/201834331](https://doi.org/10.1051/0004-6361/201834331)
- Ross, J., Latter, H. N., & Guilet, J. 2016, *MNRAS*, 455, 526, doi: [10.1093/mnras/stv2286](https://doi.org/10.1093/mnras/stv2286)
- Sano, T., Inutsuka, S.-i., Turner, N. J., & Stone, J. M. 2004, *ApJ*, 605, 321, doi: [10.1086/382184](https://doi.org/10.1086/382184)
- Sekiya, M., & Onishi, I. K. 2018, *ApJ*, 860, 140, doi: [10.3847/1538-4357/aac4a7](https://doi.org/10.3847/1538-4357/aac4a7)
- Shadmehri, M., Khajenabi, F., Dib, S., & Inutsuka, S.-i. 2018, *MNRAS*, 481, 5170, doi: [10.1093/mnras/sty2656](https://doi.org/10.1093/mnras/sty2656)
- Shakura, N. I., & Sunyaev, R. A. 1973, *A&A*, 24, 337
- Shi, J.-M., Zhu, Z., Stone, J. M., & Chiang, E. 2016, *MNRAS*, 459, 982, doi: [10.1093/mnras/stw692](https://doi.org/10.1093/mnras/stw692)
- Shu, F. H. 1977, *ApJ*, 214, 488, doi: [10.1086/155274](https://doi.org/10.1086/155274)
- Simon, J. B., Bai, X.-N., Armitage, P. J., Stone, J. M., & Beckwith, K. 2013, *ApJ*, 775, 73, doi: [10.1088/0004-637X/775/1/73](https://doi.org/10.1088/0004-637X/775/1/73)
- Stammler, S. M., & Birnstiel, T. 2022, *ApJ*, 935, 35, doi: [10.3847/1538-4357/ac7d58](https://doi.org/10.3847/1538-4357/ac7d58)
- Stammler, S. M., Birnstiel, T., Panić, O., Dullemond, C. P., & Dominik, C. 2017, *A&A*, 600, A140, doi: [10.1051/0004-6361/201629041](https://doi.org/10.1051/0004-6361/201629041)
- Taki, T., Fujimoto, M., & Ida, S. 2016, *A&A*, 591, A86, doi: [10.1051/0004-6361/201527732](https://doi.org/10.1051/0004-6361/201527732)
- Toomre, A. 1964, *ApJ*, 139, 1217, doi: [10.1086/147861](https://doi.org/10.1086/147861)
- Wada, K., Tanaka, H., Suyama, T., Kimura, H., & Yamamoto, T. 2009, *ApJ*, 702, 1490, doi: [10.1088/0004-637X/702/2/1490](https://doi.org/10.1088/0004-637X/702/2/1490)
- Woitke, P., Drazkowska, J., Lammer, H., Kadam, K., & Marigo, P. 2024, *A&A*, 687, A65, doi: [10.1051/0004-6361/202450289](https://doi.org/10.1051/0004-6361/202450289)
- Xu, W., & Kunz, M. W. 2021, *MNRAS*, 508, 2142, doi: [10.1093/mnras/stab2715](https://doi.org/10.1093/mnras/stab2715)
- Yang, C.-C., Johansen, A., & Carrera, D. 2017, *A&A*, 606, A80, doi: [10.1051/0004-6361/201630106](https://doi.org/10.1051/0004-6361/201630106)
- Youdin, A., & Johansen, A. 2007, *ApJ*, 662, 613, doi: [10.1086/516729](https://doi.org/10.1086/516729)
- Youdin, A. N., & Goodman, J. 2005, *ApJ*, 620, 459, doi: [10.1086/426895](https://doi.org/10.1086/426895)
- Youdin, A. N., & Lithwick, Y. 2007, *Icarus*, 192, 588, doi: [10.1016/j.icarus.2007.07.012](https://doi.org/10.1016/j.icarus.2007.07.012)